UNIVERSITY OF CALIFORNIA,
IRVINE

Development of Non-Invasive, Functional, Optical Imaging for Monitoring and Detecting Cardiovascular Disease

DISSERTATION

submitted in partial satisfaction of the requirements
for the degree of

DOCTOR OF PHILOSOPHY

in Biomedical Engineering

by

Robert Virgil Warren

Dissertation Committee:
Professor Bruce J. Tromberg, Chair
Associate Professor Bernard Choi
Associate Professor Elliot Botvinick

2017

DEDICATION

If I stop and think about the enormous universe and how I am just the tiniest part of it, I can't help but feel insignificant. Thankfully, the universe, instead, seems like the tiniest speck when you love something, and I am blessed to be *surrounded* by people I love. These people make it easy and exciting to wake up in the morning. My mom, dad, brother, sister, and grandparents. Terra, my rock for 5 years. Shaun, Rocky, Funshine. The Beckman Laser Institute. And without any uncertainty, my coffee-slurping, sweater junkie, know-it-all, Sephiroth-slaying, beautiful lady, Alex.

"Somewhere along the line — in one damn incarnation or another, if you like — you not only had a hankering to be an actor or an actress but to be a *good* one. You're stuck with it now. You can't just *walk out* on the results of your own hankerings. Cause and effect, buddy, cause and effect. The only thing you can do now, the only re*lig*ious thing you can do, is *act*. Act for God, if you want to — be *God's* actress, if you want to. What could be prettier? You can at least try to, if you want to — there's nothing wrong in *try*ing." There was a slight pause. "You'd better get busy, though, buddy. The goddam *sands* run out on you every time you turn around. I know what I'm talking about. You're lucky if you get time to sneeze in this goddam phenomenal world."

J.D. Salinger
"Franny and Zooey"

"My grandfather used to say: Life is astoundingly short. To me, looking back over it, life seems so foreshortened that I scarcely understand, for instance, how a young man can decide to ride over to the next village without being afraid that -not to mention accidents- even the span of a normal happy life may fall far short of the time needed for such a journey."

Franz Kafka
"The Next Village"

"Consider the subtleness of the sea; how its most dreaded creatures glide under water, unapparent for the most part, and treacherously hidden beneath the loveliest tints of azure. Consider also the devilish brilliance and beauty of many of its most remorseless tribes, as the dainty embellished shape of many species of sharks. Consider, once more, the universal cannibalism of the sea; all whose creatures prey upon each other, carrying on eternal war since the world began.
Consider all this; and then turn to the green, gentle, and most docile earth; consider them both, the sea and the land; and do you not find a strange analogy to something in yourself? For as this appalling ocean surrounds the verdant land, so in the soul of man there lies one insular Tahiti, full of peace and joy, but encompassed by all the horrors of the half-known life. God keep thee! Push not off from that isle, thou canst never return!"

Herman Melville
"Moby Dick; or, The Whale"

TABLE OF CONTENTS

LIST OF FIGURES

LIST OF TABLES

ACKNOWLEDGMENTS

Alex, Terra, my family, and my friends have spent so many years supporting me in every way imaginable. The completion of this PhD work is as much their achievement as it is mine.

Most of the concepts in this research can be traced back to my collaboration with Goutham Ganesan and he even started some of the work. In addition to thanks for getting the ball rolling with my work, he gave advice throughout the way and provided tough love when it was much needed. In the DOSI lab, many people have helped with these projects in varying degrees, so the entire lab deserves thanks. I want to point out Amanda Durkin, Brian Hill, and Drew Reilly. Amanda and Brian are the glue that holds the lab together at times and all equipment and software would be non-existent in our lab without them. Drew helped with the body composition section of this thesis and performed much of the computation. Many collaborators made this work possible by offering resources and clinical study participants, namely Josh Cotter, Shaista Malik, Tomas Stromberg, Dan Cooper, Shlomit Radom-Aizik, and Ronen Bar-Yoseph. While Goutham helped to get the ball rolling on much of my work, another colleague and friend, Abraham Chiu, helped to guide me across the finish line. Abraham welcomed me into the Pediatric Exercise Research Center and Dan Cooper's lab in the second half of my PhD tenure. It was through this collaboration that the body composition work became a reality and it provided the basis for a greater understanding of our DOSI results in biological tissue.

I have had terrific advising from Tony Durkin, Darren Roblyer, Tom O'Sullivan, Albert Cerussi, Bernard Choi, Elliot Botvinick, and Bruce Tromberg. Albert welcomed me into BLI and trained me for 2 years before I started grad school. His positivity left a mark on me and has helped to make sure I enjoy what I'm doing daily. In addition, his love for family constantly reminds me what is truly important. At a time in my life where things were basically falling apart and I probably needed a therapist rather than a PI, Tom shouldered the roll of lab director during his tenure as a post-doc at BLI. Tom helped me to understand the middle section of the PhD where "you can't see how you got in and you can't see how to get out." While he left UCI before I did manage to navigate my way out, he helped me to my feet and got me on my way.

Finally, Bruce is unquestionably the best mentor to have and I feel lucky that I could work with him for my graduate studies. Bruce is a down-to-earth, real person that can talk to you about basketball or podcasts. But he's also a visionary that can see where science is heading years down the road and will make sure we're all studying the best topics. Most importantly, for me, has been his patience. There were many times throughout grad school where we would have a meeting scheduled and I was simply not prepared to discuss anything new with Bruce. I would bring data that Bruce had seen or expected and it truly did not benefit him. And I would know that he knew that I knew that I could have done better. I could see it in his eyes. I don't truly know what happens in Bruce's mind during these moments, but what happens in the room is he asks a genuinely tough question about science and he teaches me something. He challenges me to learn and he helps me to find the next steps. He was patient with me for 5 years and I know the Herculean effort it was to get me through fellowships proposals, papers and presentations. Thanks, Bruce!

Several financial supporters also helped to make this research a reality. On an individual level, I was supported by two fellowships throughout grad school: The Cardiovascular Applied Research and Entrepreneurship fellowship from the Edwards Lifesciences Cardiovascular Center and the TL1 Pre-Doctoral fellowship from the Institute of Clinical and Translational Science, both at UC Irvine. In addition to individual fellowships, much of my work was supported by the Laser Microbeam and Medical Program, the National Institutes of Health, and the Arnold and Mabel Beckman Foundation.

CURRICULUM VITAE

Robert Virgil Warren
1002 Health Sciences Rd, Irvine, CA 92612
(949) 220-6321 • warrenr@uci.edu

Education

- PhD, Biomedical Engineering (2012 – October 2017)
  University of California, Irvine, CA
- MS, Biomedical Engineering (2012 - 2014)
  University of California, Irvine, CA
- BS, Physics (2006 - 2010)
  Harvey Mudd College, Claremont, CA

Work Experience

- Assistant Specialist, Beckman Laser Institute, UC Irvine, Irvine, CA
  (June 2012 – September 2012)
- Junior Specialist, Beckman Laser Institute, UC Irvine, Irvine, CA
  (June 2010 – June 2012)

Research Experience

- Advanced Optical Methods of Assessing Cardiovascular Disease Risk, Beckman Laser Institute, University of California, Irvine, CA (Graduate Student Researcher, September 2012 – Present)
  - Skills involved: diffuse optical spectroscopy, data processing, clinical measurements, handling patient data, designing clinical studies
  - For more information contact Bruce Tromberg - bjtrombe@uci.edu

- Monitoring Hemodynamics in Animal Models of Trauma, Beckman Laser Institute, University of California, Irvine, CA (Assistant Specialist, December 2010 – Present)
  - Skills involved: diffuse optical spectroscopy, data processing, clinical measurements, familiarity with surgical environments
  - For more information, contact Bruce Tromberg - bjtrombe@uci.edu

- Designing Fiber Optic Probes and Tissue Phantoms for Diffuse Optical Spectroscopy, Beckman Laser Institute, University of California, Irvine, CA (Junior Specialist, June 2010 – Present)
  - Skills involved: diffuse optical spectroscopy, data processing, optical fiber maintenance, making tissue phantoms
  - For more information, contact Albert Cerussi - acerussi@uci.edu

- Development of an Immunogold Labeling Technique, Harvey Mudd College, Claremont, CA (Senior thesis project, May 2009 – May 2010)
  - Skills involved: optical coherence microscopy, dynamic light scattering, immunogold labeling, PEGylation
  - For more information, contact Richard Haskell - haskell@hmc.edu

- Engineering a Matrix Material for a Tissue-engineered Cornea, Harvey Mudd College, Claremont, CA (February 2008 – May 2010)
    - Skills involved: cell culture, electrospinning, immunolabeling, confocal microscopy, scanning electron microscopy, atomic force microscopy
    - For more information, contact Elizabeth Orwin - orwin@hmc.edu

Publications in Preparation

- **RV Warren**, H Yazdi, S Telep, BJ Tromberg, T Stromberg. “Simultaneous Assessment of Deep and Superficial Oxygen Saturation and Blood Flow During Vascular Reactivity Assessments.”
- **RV Warren**, A Chiu, R Bar-Yoseph, S Aizik, D Cooper, BJ Tromberg. "Diffuse Optical Spectroscopic Assessment of Body Composition and Comparisons with DXA.”

Publications

- T O’Sullivan, K No, A Matlock, **RV Warren**, B Hill, A Cerussi, BJ Tromberg. “Vertical-cavity surface-emitting laser (VCSEL) sources for gigahertz-bandwidth, multi-wavelength frequency domain photon migration.” In press at Journal of Biomedical Optics.
- **RV Warren**, J Cotter, G Ganesan, L Le, JP Agustin, B Duarte, K Cutler, T O’Sullivan, BJ Tromberg. “Non-invasive Optical Imaging of Resistance Training Adaptations in Human Muscle.” Submitted to Journal of Biomedical Optics on 24 August 2017.
- Ganesan, GG, **RV Warren**, A Leproux, M Compton, K Cutler, S Wittkopp, G Tran, T O'Sullivan, S Malik, P Galassetti, B Tromberg. “Diffuse optical spectroscopic imaging of subcutaneous adipose tissue metabolic changes during weight loss.” International Journal of Obesity, Vol. 40, Issue 8, (2016).
- Roblyer, D, TD O'Sullivan, **RV Warren**, BJ Tromberg. "Feasibility of Direct Digital Sampling for Diffuse Optical Frequency Domain Spectroscopy in Tissue." Measurement Science and Technology, Vol. 24, Issue 4, (2013).
- Cerussi, AE, **RV Warren**, B Hill, D Roblyer, A Leproux, AF Durkin, TD O'Sullivan, S Keene, H Haghany, T Quang, WM Mantulin, and BJ Tromberg. "Tissue Phantoms in Multicenter Clinical Trials for Diffuse Optical Technologies." Biomedical Optics Express, Vol. 3, Issue 5, pp. 966-971 (2012).
- Phu, D, L Wray, **RV Warren**, E Orwin, and R Haskell, "Effect of Substrate Composition and Alignment on Corneal Cell Phenotype." Tissue Engineering Part A, Vol. 17, Issue 5, pp. 799-807 (2011).

Patents

- **RV Warren**, G Ganesan, T O’Sullivan, S Malik, BJ Tromberg, P Galassetti. “Predicting Weight Loss and Fat Metabolism Using Optical Signal Changes in Fat.” Filed January 20, 2017. US Patent Application 20170209089 A1.

Proceedings Papers

- Ganesan, G, W Reuland, **RV Warren**, SM Zarandi, AE Cerussi, BJ Tromberg, PR Galassetti. “Use of diffuse optical spectroscopy to monitor muscle and brain oxygenation dynamics during isometric and isokinetic exercise. Proceeding of SPIE Vol. 8578: Optical Tomography and Spectroscopy of Tissue X. 2013.

- Keene, ST, AE Cerussi, **RV Warren**, B Hill, DM Roblyer, A Leproux, AF Durkin, TD O'Sullivan, H Haghany, WW Mantulin, BJ Tromberg. "Development of Quality Control and Instrumentation Performance Metrics for Diffuse Optical Spectroscopic Imaging Instruments in the Multi-Center Clinical Environment." Proceeding of SPIE Vol. 8578: Optical Tomography and Spectroscopy of Tissue X. 2013.

Professional Presentations

- "Monitoring Resistance Training with Diffuse Optical Spectroscopic Imaging." **RV Warren**, J Cotter, G Ganesan, B Duarte, K Cutler, T O'Sullivan, BJ Tromberg. SPIE Photonics West – BIOS. 1 February 2017.
- SPIE Photonics West 2015 Poster: "Monitoring the Effect of Strength Training on Muscle Structure and Metabolism with Diffuse Optical Spectroscopy," **RV Warren.**
- Gordon Research Conference, Biology & Pathobiology of the Cornea 2010 Poster: "Development of an Immunogold Labeling Technique for Analyzing a Tissue-Engineered Corneal Equivalent," **RV Warren.**
- Tissue Engineering & Regenerative Medicine International Society NA 2008 Poster: "Replicating the Corneal Microstructure Using Chondroitin Sulfate," **RV Warren.**

Fellowships & Honors

- NIH TL1 - Institute of Clinical and Translational Science Pre-Doctoral Fellow, ICTS, UC Irvine, CA
  (March 2016 – present)
- Accepted into the 7th International Graduate Summer School for Biophotonics '15
- NIH T32 - Cardiovascular Applied Research and Entrepreneurship Fellow, Edwards Lifesciences Center for Advanced Cardiovascular Technology, UC Irvine, CA
  (April 2013 – May 2015)

Teaching, Lecturing, and Mentoring Experience

- Lead Mentor for Summer Pathways to Biophotonics and Biomedical Engineering Program at UC Irvine (Summer 2017)
- Teaching Assistant at UC Irvine, "Biomedical Engineering Senior Design."
  (2015 – 2016)
- "Biomedical Engineering: Application of Light and Optics for Biological and Medical Applications." Joint lecture between Bernard Choi, **Robert Warren**, Caitlin Regan. Irvine Unified School District 21st Century Career Conference. 14 December 2016.
- "An Introduction to DOS: Identifying the Diffuse Optical Spectroscopic Signatures of Cardiovascular Disease." **RV Warren**. Invited lecture to visiting Linköping University research group. 14 October 2016.
- I have mentored several high school students, in addition to three undergraduate students and one graduate student for the following projects:
  - Diffuse optical spectroscopic methods of hydration and fat content monitoring
    Master's thesis – (January 2016 - Present)
  - Analysis of endothelial function in healthy individuals
    Undergraduate research – (October 2015 - Present)
  - Design and fabrication of arm-rest with embedded optical probes for clinical assessments
    Undergraduate research – (February 2016 – August 2016)

- Development of tissue-simulating phantoms
  Undergraduate research – (2011 - 2013)

Additional Skills

- Data analytics and modeling with MATLAB
- Experience with traditional bio-statistical methods
- Currently developing machine learning skills (Coursera)
- Experience in writing and modifying clinical research protocols for IRB approval
- Software Proficiencies: ZEMAX, R, MS Office
- Basic programming in Python, C++, C#
- Hobbyist experience with Arduino projects (C++ programming and basic hardware)
- Language: Elementary Italian and Spanish
- Trained to use Virtual Tissue Simulator (http://www.virtualphotonics.org/vts/) for light-tissue interaction modeling

ABSTRACT OF THE DISSERTATION

Development of Non-Invasive, Functional, Optical Imaging for Monitoring and Detecting Cardiovascular Disease

By

Robert Virgil Warren

Doctor of Philosophy in Biomedical Engineering

University of California, Irvine, 2017

Professor Bruce J. Tromberg, Chair

Cardiovascular disease (CVD) is the number one killer in the world, yet one third of CVD-related deaths occur in asymptomatic individuals and one fifth of these individuals bear no previous diagnosis of CVD [1]. New methods that provide a better understanding of CVD risk factors and detect asymptomatic disease could save many lives. In this work, I introduce diffuse optical spectroscopic imaging (DOSI) as a new method for non-invasively assessing “silent” CVD and CVD risk. DOSI is a quantitative, model-based technique that utilizes a broadband wavelength range, corrects for light scattering, and probes several centimeters into tissue. DOSI is particularly relevant for cardiovascular disease research because it measures absolute concentrations of the primary light absorber in blood, hemoglobin, as well as the oxygenation state of hemoglobin, lipid content, and water content. These features of DOSI allow for hemodynamic measurements, compositional analysis, and reliable comparisons across operators, instruments, and even separate institutions.

I demonstrate a diffuse optical spectroscopic vascular health assessment which samples three important features of vascular health: *body composition*, *tissue metabolism*, and *vascular reactivity*. In a pilot study of body composition assessment, DOSI is used to track alterations in human muscle tissue following 5-weeks of resistance training. These assessments of muscle are compared to dual-energy x-ray absorptiometry (DXA), a standard body composition assessment technique. A similar approach is used in a study of 103 individuals but is extended to sample the whole body. Using DOSI assessments at 12 anatomical locations, a method is developed to predict whole-body fat and lean soft tissue percentage. Next, I study hemodynamics in a cohort of healthy volunteers using a vascular occlusion technique. This study characterizes the range of tissue metabolism we expect to see in healthy individuals and identifies how adipose tissue thickness affects DOSI assessments. Finally, preliminary data on vascular reactivity from patients with confirmed vascular disease is presented and I propose a framework for future vascular health assessments with DOSI.

1) INTRODUCTION

The development of cardiovascular disease (CVD) takes place with a long asymptomatic period, so large potential exists for reducing deaths and medical costs through early detection and risk assessment. Cost-efficient methods to non-invasively measures early signs of CVD can have significant impact. While new risk assessment methods must be validated in large cohorts over many years, we can develop and characterize the ability of promising techniques to sense the presence and regression of diseases right now. This can be accomplished, for example, by comparing known populations with and without CVD and by monitoring the effects of short-term interventions which are known to reduce the risk and progression of CVD. This project focuses on an advanced technology in biomedical optics called diffuse optical spectroscopic imaging (DOSI), which has the potential to provide new, cost-effective methods for evaluating CVDs. At least three physiological features relevant to CVD can be assessed with DOSI: composition, metabolism, and vascular reactivity. The presence of lean and strong muscle is a good indicator of overall health and we can monitor exercise training with DOSI. In addition, the prevalence of metabolic syndrome and the obesity epidemic suggest that we also need tools which can characterize an individual's tissue and whole-body metabolism. Finally, by analyzing hemodynamics during vascular occlusion tests, DOSI can specifically study the functional health of the vascular endothelium. These three measurements are not part of the current CVD risk assessment recommended by cardiologists, but this is primarily due to limited access to technology and limited data validating the use of these tests [2]. This project aims to address these limitations and assess the suitability of DOSI for use in evaluating the

presence, regression, and progression of CVD. The long-term goal of this study will be to translate these DOSI devices into more common use in cardiovascular care.

1.1) The Burden of Cardiovascular Disease

In the 2011 World Health Organization report about worldwide causes of death, three of the top ten causes of death are intimately related to cardiovascular health: ischemic heart disease, stroke, and diabetes [3]. In 2003, the monetary costs of cardiovascular disease and diabetes in the U.S. population were $351.8 billion and $132.0 billion [4]. The American College of Cardiology Foundation and the American Heart Association periodically release updated guidelines for the risk assessment of CVD. In the most recent edition regarding asymptomatic individuals, known risk assessment techniques are broken down into several categories: global risk scoring (includes what are known as "classic risk factors"[1]), family history and genomics, lipoprotein and apolipoprotein assessments, other circulating blood markers and associated conditions, cardiac and vascular tests, and special circumstances and other considerations [2]. A summary of the recommendations by the authors is provided in the appendix (Table A1).

While patients showing symptoms of CVD represent a major portion of those who die from CVD, almost half of coronary deaths occur with no reported symptoms or previous diagnoses [2]. Major steps have been taken in the last few decades to advance risk assessment for CVD and evidence suggests that 44% of the decrease in CVD deaths between 1980 and 2000 is due to changes in risk factors [2]. There is a

[1] "Classic risk factors" are recognized as cigarette smoking, cholesterol levels, blood pressure levels, and diabetes status.

long asymptomatic period during the development of CVDs, so novel methods to non-invasively assess CVD risk with cost-efficient technologies can have significant impact by allowing individuals to affect their cardiovascular status much earlier. This project proposes that advanced optical methods have the potential to enhance risk assessment and should be translated into use in cardiovascular care.

1.2) A Paradigm for Using Diffuse Optics in Vascular Health Assessments

All problems in medicine rely on knowledge of the structure and function of biological tissue. Samples of tissue can be collected via biopsy, but a non-invasive technique such as imaging is almost always preferable. The near-infrared spectrum of light presents an ideal method for probing several centimeters deep into tissue with non-ionizing light. The primary light absorbing components of biological tissue are hemoglobin, water, and fat, all of which absorb minimal amounts of light from the near-infrared region compared to the rest of the electromagnetic spectrum [5].

Aside from absorption events which affect photons traveling through tissue, scattering also takes place. The most accurate method of describing photon travel through tissues comes from Maxwell's equations of electromagnetism, but approximate methods have been developed to model photon travel in biological tissue with relative ease. An excellent background on these models can be found in Haskell et al.'s pivotal work on photon diffusion theory [6], and a brief review of the theory relevant to this work will be covered in Chapter 2.

In our case, the goal of any type of photon transport model is the extraction of absorption and scattering properties of biological tissue. In model-based optical

methods where absorption and scattering events can be separated, the measured absorption spectra of bulk biological tissue can be decomposed into component spectra so concentrations of individual components can be determined. DOSI, the technology used throughout this thesis, is an example of such a method [7].

2) DIFFUSE OPTICAL SPECTROSCOPIC IMAGING (DOSI)

2.1) Introduction to Light-Tissue Interactions

The use of light for biomedical applications necessitates a careful understanding of how photons behave once they enter biological tissue. Photons can experience scattering and absorption within tissue and reflection and transmission at tissue boundaries. The field of study which focuses on these processes is known as tissue optics and a basic understanding of the core concepts helps to understand latter parts of this thesis.

In tissue optics, we define the scattering coefficient (μ_s) and absorption coefficient (μ_a) as the inverse of the mean free path for scattering and absorption. These parameters are useful when a biochemical description of a tissue's structure and composition is desired. If we focus on a tissue's scattering characteristics, for example, light will experience scattering at different rates as it travels through tissue. Not only will tissue constituents scatter light in unique ways, but the wavelength of light also determines how it experiences scattering inside of tissue. In most biological tissues, Mie scattering is the dominant form of scattering and the wavelength dependence of scattering follows a predictable form:

$$\mu_s'(\lambda) = A \times \left(\frac{\lambda}{500\ nm}\right)^{-b}$$

where λ is the wavelength of light, A is the scattering amplitude, b is the scattering power, and the denominator is a scaling factor which is used to more easily understand results near commonly used wavelengths of light [5].

In addition to light scattering, light can experience absorption. The absorption coefficient, μ_a, is mathematically defined as

$$\mu_a = -\frac{1}{T}\frac{\partial T}{\partial L}$$

where T (dimensionless) is the transmitted fraction of incident light which successfully passes through an incremental pathlength, ∂L. Solving for T in terms of L, we can write

$$T = e^{-\mu_a L}.$$

An alternative means for describing the transmitted fraction of light is with an extinction coefficient, such as

$$T = 10^{-\varepsilon C L}$$

where C is the concentration of a chromophore and ε is the extinction coefficient of the chromophore. Setting these two equations for T equal, we can solve for μ_a in terms of C and ε,

$$\mu_a = \ln(10) \times C\varepsilon = 2.303 \times C\varepsilon.$$

Rearranging this equation, we have a way to calculate the concentration of a chromophore given a measured μ_a and previously known ε,

$$C = \frac{\mu_a}{2.303}\frac{1}{\varepsilon}.$$

If multiple absorbing chromophores are present in a given tissue, their absorption behaviors are additive and a medium's total absorption can be represented as a linear combination of absorbers:

$$tissue\ \mu_a = \ln(10) \sum_{i=1}^{n} C_i \varepsilon_i.$$

We can solve for the vector of unknown concentrations, C_i, given known extinction coefficients, ε_i, and a measured tissue absorption, $tissue\ \mu_a$, by employing matrix inversion or a least-squares computational approach. Thus, it is possible to solve for concentrations of several absorbers if a corresponding number of distinct wavelengths of light are utilized.

A natural question at this point is: which wavelengths of light should we use to study biological tissue? The near-infrared (NIR) spectrum of light is a popular choice since light attenuation due to absorption is minimal and photons can probe several centimeters into and back out of tissue (Figure 1) [5]. The 600 – 1000 nm range is commonly known as the “near-infrared window” and is utilized for studying deep into biological tissue. In addition to allowing deep tissue analysis, the NIR range of light is primarily affected by several absorbers of light which are highly relevant to medicine: heme proteins (e.g. hemoglobin and myoglobin), lipids, and water. Each of these components have unique spectral absorption properties and can readily be separated and quantified using the analysis techniques described above.

The primary challenge when studying scattering and absorption characteristics of tissue is that both effects result in attenuation of light and are difficult to distinguish. The ability to shine light into biological tissue and uniquely quantify the defining scattering and absorption rates of the tissue is a difficult problem and will be discussed in the next section.

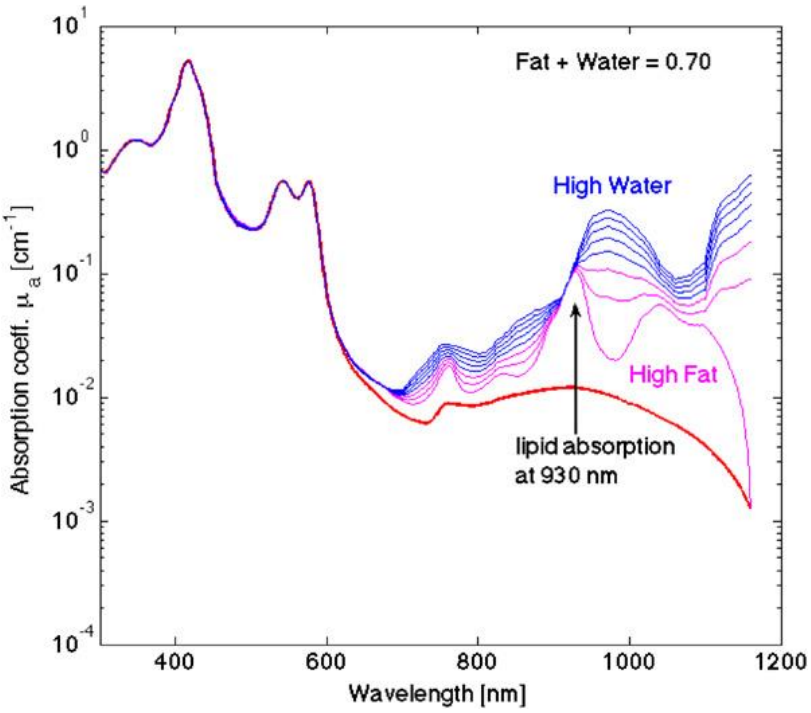

Figure 1. Borrowed from Jacques 2013. This plot shows the absorption spectrum of a typical biological tissue. In the visible wavelengths (<600 nm), hemoglobin absorbs light at high rates whereas water and fat absorb light at high rates as you venture further into the infrared (>1000 nm). The "near-infrared window" is between 600 – 1000 nm [5].

2.2) Frequency Domain Photon Migration (FDPM)

As described in the previous section, uniquely describing the scattering and absorption behaviors of a biological tissue can have important implications for biomedical optics. For this purpose, we will describe a technique known as frequency domain photon migration (FDPM) which allows for quantitative determinations of the reduced scattering coefficient (μ_s') and absorption coefficient (μ_a) of a tissue.

Boltzmann Transport Equation

A complete treatment of light propagation in biological tissue requires the use of Maxwell's equations of electromagnetism. However, the large degree of scattering in biological tissue leads to a complex superposition of waves and boundary conditions which are exceedingly difficult to solve with both analytical and numerical solvers [7]. A simplified approach involves the treatment of light as noninteracting particles, whereby the Boltzmann transport equation suffices to describe light transport in tissue [6]. The Boltzmann transport equation is formalized as

$$\frac{1}{c}\frac{\partial L(\boldsymbol{r},\hat{s},t)}{\partial t} + \boldsymbol{\nabla}\cdot L(\boldsymbol{r},\hat{s},t)\hat{s} =$$

$$-(\mu_s+\mu_a)L(\boldsymbol{r},\hat{s},t) + \mu_s \iint_{4\pi} L(\boldsymbol{r},\hat{s}',t) f(\hat{s}\cdot\hat{s}')\, d\Omega' + Q(\boldsymbol{r},\hat{s},t),$$

where $c = (3{\times}10^8 m/s)/n$ is the speed of photons in a biological tissue of refractive index n, $L(\boldsymbol{r},\hat{s},t)$ is radiance which has units of W/(m^{2}sr), $\hat{s}$ is a unit vector pointing in a given direction, $f(\hat{s}\cdot\hat{s}')$ is the normalized differential scattering cross section which satisfies

$$\iint_{4\pi} f(\hat{s}\cdot\hat{s}')\, d\Omega' = 1,$$

and $Q(\boldsymbol{r},\hat{s},t)$ is a source term which injects light power into a unit solid angle centered on $\hat{s}$ in a unit volume at $\boldsymbol{r}$ [6]. If we integrate over all solid angles, the Boltzmann transport equation can be rewritten as

$$\frac{1}{c}\frac{\partial \phi(r,t)}{\partial t} + \boldsymbol{\nabla}\cdot \boldsymbol{j}(\boldsymbol{r},t) = -\mu_a \phi(\boldsymbol{r},t) + S(\boldsymbol{r},t),$$

where

$$S(\boldsymbol{r},t) \equiv \iint_{4\pi} Q(\boldsymbol{r},\hat{s},t)\, d\Omega,$$

$$\phi(\boldsymbol{r},t) \equiv \iint_{4\pi} L(\boldsymbol{r},\hat{s},t)\, d\Omega,$$

$$\boldsymbol{j}(\boldsymbol{r},t) \equiv \iint_{4\pi} L(\boldsymbol{r},\hat{s},t)\hat{s}\, d\Omega.$$

The terms $\phi(\boldsymbol{r},t)$ and $\boldsymbol{j}(\boldsymbol{r},t)$ are fluence rate and flux, respectively [6].

The Diffusion Approximation

If scattering takes place at a much higher rate than absorption ($\mu_s' \gg \mu_a$), a diffusion approximation can be made and radiance can be described as an isotropic fluence rate with a small directional flux:

$$L(\boldsymbol{r},\hat{s},t) = \frac{1}{4\pi}\phi(\boldsymbol{r},t) + \frac{3}{4\pi}\boldsymbol{j}(\boldsymbol{r},t)\cdot\hat{s}.$$ [6]

With the diffusion approximation made, we can substitute this form of radiance back into the Boltzmann transport equation, multiply by $\hat{s}$, and integrate over all solid angles to obtain

$$\frac{1}{c}\frac{\partial \boldsymbol{j}(\boldsymbol{r},t)}{\partial t} = -\frac{1}{3}\boldsymbol{\nabla}\phi(\boldsymbol{r},t) - \frac{1}{3D}\boldsymbol{j}(\boldsymbol{r},t)$$

where the diffusion coefficient, D, is defined as

$$D \equiv \frac{1}{3[(1-g)\mu_s+\mu_a]} \equiv \frac{1}{3\mu_s'}$$ [6].

During steady state, we can solve for flux, $\boldsymbol{j}(\boldsymbol{r},t)$, where the resulting equation is the famous Fick's law:

$$\boldsymbol{j}(\boldsymbol{r},t) = -D\boldsymbol{\nabla}\phi(\boldsymbol{r},t).$$

Although this equation for flux was derived for a steady state source, it is still a reasonable approximation in biological tissue when the source varies at frequencies lower than ~1 GHz [6]. This relation between the flux and fluence rate allows us to rewrite our differential equation in terms of the fluence rate alone:

$$D\boldsymbol{\nabla}^2\phi(\boldsymbol{r},t) - \mu_a\phi(\boldsymbol{r},t) =$$

$$(1 + 3D\mu_a)\frac{1}{c}\frac{\partial\phi(\boldsymbol{r},t)}{\partial t} - S(\boldsymbol{r},t) + \frac{3D}{c^2}\frac{\partial^2\phi(\boldsymbol{r},t)}{\partial t^2} - \frac{3D}{c}\frac{\partial S(\boldsymbol{r},t)}{\partial t}.$$

Given the much higher rate of scattering than absorption in biological tissue, we can neglect the term $3D\mu_a$. Finally, as we have restricted this description to sources which vary slower than 1 GHz, the final two terms can also be neglected and we are left with the diffusion equation

$$D\boldsymbol{\nabla}^2\phi(\boldsymbol{r},t) - \mu_a\phi(\boldsymbol{r},t) = \frac{1}{c}\frac{\partial\phi(\boldsymbol{r},t)}{\partial t} - S(\boldsymbol{r},t)$$ [6].

Solving the Diffusion Equation for a Harmonic Source

The solution to this diffusion equation for a harmonic source at the origin emitting power $P = e^{i\omega t}$ is known as a "photon density wave" and takes the form

$$\phi(\boldsymbol{r},\omega,t) = \frac{P}{4\pi D}e^{-k_{real}r}\frac{e^{-i(k_{imag}r-\omega t)}}{r}$$

where the k wave vector

$$k = k_{real} + ik_{imag} = \sqrt{\frac{\mu_a c+i\omega}{Dc}}$$, and $\tau \equiv \frac{1}{\mu_a c}$

such that

$$k_{real} = \sqrt{\frac{3}{2}\mu_a\mu_{tr}}\left[\sqrt{1+(\omega\tau)^2}+1\right]^{1/2},$$

$$k_{imag} = \sqrt{\frac{3}{2}\mu_a\mu_{tr}}\left[\sqrt{1+(\omega\tau)^2}-1\right]^{1/2}$$ [6].

In the above equations, τ is defined as the absorption relaxation time.

Practical Application of FDPM Theory

In practice, a light source will contain AC and DC components in the following form:

$$\phi(\boldsymbol{r}, \omega, t) = A_{DC} \frac{e^{-r/\delta}}{r} + A_{AC} \frac{e^{-k_{real} r}}{r} e^{-i(k_{imag} r - \omega t)},$$

where δ is the DC attenuation length and can be derived by setting $\omega = 0$ in the expression for k_{real} [6]. With a detector placed a distance r away from the source and oriented perpendicular radial flux of the source, the detected signal will be proportional to the source fluence rate but with a phase lag given the distance from the source $phase\ lag = k_{imag} r$ [6].

In addition to a phase lag, the detected signal will have a reduced modulation amplitude relative to the source given by

$$modulation = \left[A_{AC} \frac{e^{-k_{real} r}}{r} \Big/ A_{DC} \frac{e^{-r/\delta}}{r} \right] \Big/ \left[A_{AC} / A_{DC} \right]$$ [6].

The phase lag and modulation are the primary outputs from FDPM and fitting measured data against this modeled behavior allows for the determination of μ_a and μ_s'.

Semi-infinite Boundary Condition and Non-invasive Tissue Measurements

A final extension of this theory in practice is the implementation of a semi-infinite boundary condition to more accurately describe photon transport when a non-invasive tissue measurement is performed (accounting for the air/tissue interface). Several approaches have been described for this process, but our lab uses the extrapolated-boundary condition approach described by Haskell et al [6]. This approach leads to a fluence rate solution of the form

$$\phi(\rho, z, \omega, t) = A_{DC}\left[\frac{e^{-r_1/\delta}}{r_1} - \frac{e^{-r_b/\delta}}{r_b}\right] + A_{AC}\left[\frac{e^{-kr_1}}{r_1} - \frac{e^{-kr_b}}{r_b}\right]e^{i\omega t},$$

where ρ, r_1, and r_b are geometrical features of the extrapolated-boundary setup, as well as modified formulations for the detected phase lag and modulation which can be seen in their work [6].

2.3) Broadband Diffuse Optical Spectroscopy (DOS)

With a determination of μ_a and μ_s' from FDPM, we can solve for concentrations of chromophores inside of biological tissue. Our only constraints are that the basis spectra for absorbing chromophores must be linearly independent and we must have resulting μ_a for as many distinct wavelengths as there are chromophores. As an example, if we wish to solve for concentrations of oxy- hemoglobin, deoxy-hemoglobin, fat, and water, we need a minimum of four wavelengths and they must be spectrally located where each chromophore absorbs light in a unique way (e.g. 750 nm, 850 nm, 930 nm, 970 nm). While technically feasible, the approach described by Bevilacqua et al. combines FDPM with a steady-state reflectance method and theoretically allows for broadband characterization of μ_a at hundreds of wavelengths [8].

Steady-state reflectance is affected by both μ_a and μ_s' and when measured at a single source-detector separation we cannot determine μ_a. We recall, however, that the wavelength dependence of scattering is a smooth, predictable function (CITE MIE ABOVE) [5]. If we determine μ_s' at enough wavelengths to resolve this wavelength dependence, we can fit our FDPM results to the power law dependence and obtain broadband μ_s'. Finally, we can leverage this information along with steady-state,

broadband reflectance to determine broadband μ_a at hundreds of wavelengths, namely across the NIR window (650 – 1000 nm).

In all studies described below, we have utilized this combination of SS and FDPM methods in a single instrument and technique we term diffuse optical spectroscopic imaging (DOSI). A single measurement on human tissue takes ~1-5 seconds and the primary result is broadband μ_a and μ_s' which represents a deep (~1 cm) bulk characterization of tissue.

3) OPTICAL BODY COMPOSITION ASSESSMENT

3.1) Tissue Composition: A Pilot Study in Resistance Training

3.1.1) Introduction

Skeletal muscle plays a major role in whole-body protein stability and maintenance and is an important measure of an individual's ability to maintain overall health, optimize athletic performance, and overcome injury [9-11]. Researchers have also demonstrated correlations between decreased muscle mass and strength with obesity, chronic diseases such as heart failure and cancer, the development of insulin resistance and diabetes, and osteoporosis [12]. As a result, the development of quantitative, bedside, and wearable technologies for characterizing muscle composition and assessing long-term changes and interventions would be broadly impactful in precision medicine and personal health.

A common tool in muscle assessment is dual-energy x-ray absorptiometry (DXA). DXA can non-invasively scan the body and quantify composition, i.e. the amount of fat, lean soft tissue, and bone mineral content present in specific tissue

compartments [13]. Despite the utility of DXA measurements, DXA machines are not portable and are unable to assess perfusion and oxygen saturation, both of which are important in exercise and health assessments. In addition, a measurement of lean soft tissue mass is not a direct means of quantifying muscle mass as it is the "residual" component in DXA's three component model of fat tissue, bone mineral, and residual lean soft tissue [13].

In contrast, near-infrared spectroscopy (NIRS) is portable and can be tailored to study muscle physiology in many experimental paradigms, as described in several reviews [14-16]. NIRS has also been used to study hemodynamics in muscle for several decades [17]. Studies during the 2000s developed mapping/imaging techniques for assessing the spatial variations of muscle during rest and exercise [18, 19]. More recent studies have focused on combining NIRS with diffuse correlation spectroscopy to assess oxygen saturation of the muscle as well as blood flow [20, 21]. NIRS can also be utilized to track water and lipid content in biological tissue [22]. While the relationship between neural and hypertrophic strength gains is well characterized in older literature and hypertrophy is thought to occur after 6-7 weeks of exercise [23, 24], recent studies have shown that hypertrophy might take place in as little as 3-4 weeks of training [25, 26]. However, early increases in muscle cross-sectional area may be due to edema-induced swelling [27]. As such, the water and lipid monitoring capabilities of NIRS could be useful in monitoring early resistance-training studies.

In this work, we evaluate whether a form of NIRS, broadband diffuse optical spectroscopic imaging (DOSI,) can be used to quantitatively assess long-term changes in intrinsic tissue composition following resistance training (RT). DOSI combines

frequency domain photon migration (FDPM) with time-independent broadband NIRS to separate light scattering from absorption in centimeter-thick tissues. Scatter-corrected absorption spectra are used to calculate the tissue concentration of oxygenated and deoxygenated hemoglobin/myoglobin as well as water and lipid content. Because spectra are acquired using a handheld probe, DOSI can form topographic maps and reveal spatial variations in tissue properties [7].

DOSI has been used extensively as a long-term monitoring technology in breast cancer where levels of water, lipid, and hemoglobin change over the course of 3-6 months of chemotherapy [28-30]. We have also used DOSI to monitor changes in adipose tissue as patients underwent 3-months of calorie-restriction weight loss [22]. In addition, the ability of DOSI to reliably measure water and lipid content has been validated in a study using magnetic resonance imaging (MRI) [31]. It seems likely that DOSI could provide useful information for body composition analysis since it is able to quantify levels of blood, water, and fat in tissue. For this purpose, we test for associations between DOSI-measured tissue chromophores and DXA-measured fat and lean soft tissue mass. We hypothesized that correlations would exist between these distinct methods of tissue composition assessment, with a high lean/fat mass ratio from DXA correlating with DOSI measurements of increased hemo+myoglobin and water (i.e. lean mass) and less lipid (i.e. fat mass). In addition, we attempted to identify which DOSI parameters are sensitive to tissue adaptations that accompany resistance training. Unlike previous NIRS muscle studies that primarily track hemodynamic changes during and immediately post-exercise, we report, for the first time, how DOSI

can be used to assess long-term changes in calf muscle composition over a period of 5 weeks.

3.1.2) Methods

3.1.2.1) *Participants and experimental design*

A total of 15 participants (9 males and 6 females; 20.9 ± 3.8 yr, 65.7 ± 10.4 kg, 168.6 ± 7.3 cm) were recruited for the study. Participants were non-smokers who were not involved in any athletic or programmed physical activities for the previous six months, had no history of asthma, cardiopulmonary, or musculoskeletal disease, and were not currently taking any medications or sports supplements. Training and testing took place in the Human Performance Laboratory of the Institute for Clinical and Translational Science (ICTS) at the University of California, Irvine. Participants provided written informed consent before their involvement in the study. Following consent, two of three exercise protocols (see Exercise Training below) were randomly assigned to each participant with one protocol being applied to the left leg and a second, different protocol applied to the right leg using a block-randomization schedule. Participants attended two to three preliminary sessions to be familiarized with the testing and training equipment. Following familiarization, testing measurements were performed during a baseline session before exercise training began and a post-training session following five weeks of exercise training. Each testing session included body composition assessed by DXA and DOSI. In addition to these assessments, muscular strength was determined using a one repetition maximum (1RM) model. The study

protocol was approved in advance by the Institutional Review Board of the University of California, Irvine.

3.1.2.2) *Exercise Training*

Resistance training occurred over a five-week period with participants training three days per week for total of 15 training sessions. This study utilized three exercise training protocols: 1) low-intensity at 20% 1RM (LIT), 2) high-intensity exercise @ 70% 1RM (HIT), and 3) low-intensity exercise at 20% 1RM with blood-flow restriction (LIT+BFR). Exercise training occurred unilaterally on a 45-degree angle hack squat machine (HF-4357, Hoist Fitness, San Diego, CA). Participant foot placement was determined by centering the metatarsophalangeal articulation for the sagittal plane and the medial side of the shoe for the frontal plane on the equipment foot plate. During each session, the right leg was trained first followed by the left leg. Each repetition started with the ankle in a dorsiflexed position. Participants were encouraged to plantar flex under maximal effort with a controlled descent back to the initial dorsiflexed position for 1.5 seconds controlled with a metronome. Under the protocol with BFR, an automated blood pressure cuff (Hokanson, Inc., Bellevue, WA, USA) was placed proximal to the knee joint during training. The cuff was inflated to 1.3 x systolic blood pressure before the commencement of exercise. Following the training session, participants consumed 20 grams of high-quality whey protein supplement (Optimum Nutrition, Downers Grove, IL, USA) in 200 mL of water.

3.1.2.3) *1-Repetition Maximum (1RM) Strength Testing*

Participants were positioned on the exercise equipment and instructed by study personnel to perform exercises at maximal exertion utilizing the technique described above. A repetition was considered successful if the distance the weight was lifted equated to at least 80% of the maximum distance obtained during an unloaded repetition. Following a successful repetition, participants rested at least 1.5 minutes before weight was incrementally increased in association with guidelines set forth by the National Strength and Conditioning Association [32]. Incremental increases were repeated until a participant was unable to perform a successful repetition. The highest load lifted for a successful repetition was noted as the participant's 1RM.

3.1.2.4) *Dual Energy X-Ray Absorptiometry (DXA) Measurements*

DXA measurements were performed at baseline and post-training with a Hologic Discovery A DXA system using Apex 3.3 software (Hologic, Marlborough, MA, USA). Participants laid supine on a padded table with all metal objects removed. Participants were raster scanned from head to foot and then the lower leg region was defined superiorly by tibiofemoral joint and inferiorly by the talocrural joint. To more directly compare DOSI and DXA values, bone mineral content was excluded from the DXA data and only soft-tissue parameters were analyzed. Specifically, soft-tissue is comprised of fat mass (FM) and residual lean soft tissue mass (LM). In addition to FM and LM, the fraction of the soft tissue that is LM is defined in this study as lean mass fraction (LMF).

3.1.2.5) *Diffuse Optical Spectroscopic Imaging (DOSI) Measurements*

The technical details of DOSI have been described previously [7]. Briefly, DOSI combines frequency domain photon migration (FDPM) and broadband spectroscopy to obtain absorption and scattering coefficients across a broad range of wavelengths (650 – 1000 nm). This allows for precise quantitation of tissue concentrations of the major absorbers in this range of wavelengths. The system used in this study has been described previously but a brief overview will be provided here [22]. The FDPM system utilizes three intensity-modulated near infrared (NIR) laser diodes (690, 785, and 835 nm) and an avalanche photodiode detector to collect diffusely reflected light in the form of photon density waves. The broadband NIRS system utilizes a broadband quartz tungsten halogen (QTH) source and a spectrometer for light collection. All light sources are fiber-coupled into a handheld probe that contains the avalanche photodiode and another optical fiber coupled to a spectrometer. Fiber placement in the probe allows for co-registered FDPM and broadband NIRS measurements with a source-detector separation that is fixed at 28 mm.

DOSI measurements were performed at baseline and post-training. Post-training DOSI assessments were performed at least 65 hours (80 +/- 13 hours) following the final exercise session for all participants. Participants were positioned prone on a padded table and grids of 48 points each were drawn over both calves (Figure 2). The grids consisted of 6 rows and 8 columns, each separated by 2.5 cm (~220 cm^2 total area). Three broadband DOSI scans were performed (approximately 3 seconds per scan) at each grid point and tissue chromophore concentrations were averaged from the sequential scans. The chromophores analyzed in this study consisted of oxygenated hemo+myoglobin ($HbMbO_2$), de-oxygenated hemo+myoglobin (HbMbR),

water content (Water), lipid content (Lipid), and then the following derived parameters: total hemo+myoglobin (THbMb = $HbMbO_2$+HbMbR) and oxygen saturation (StO_2 = $HbMbO_2$/THbMb).

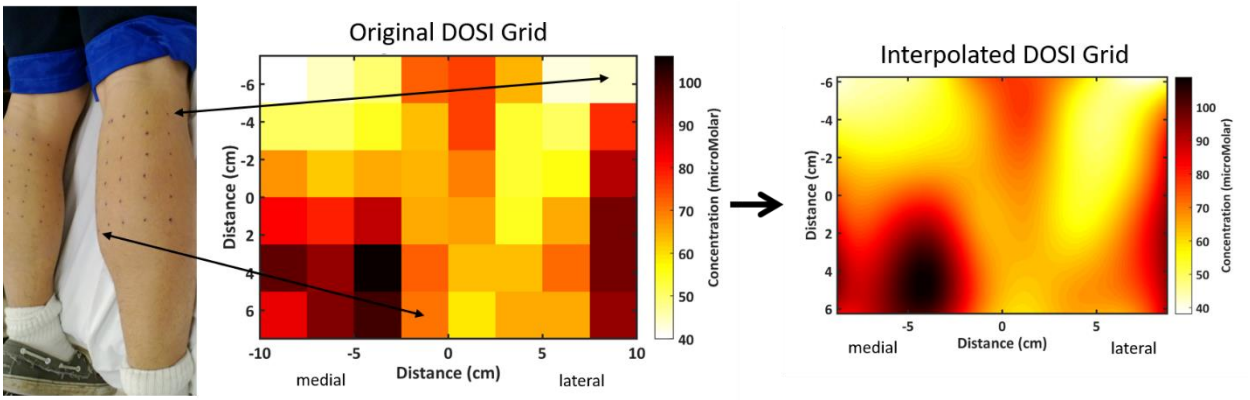

Figure 2. The photo on the left shows a sample participant with the DOSI grid-points on the lower legs. Eight columns and six rows covered each leg, with each point being spaced 2.5 cm from the next point. DOSI THbMb results are shown in a grid image in the middle. On the right, an interpolated DOSI image is formed by using cubic spline interpolation between points. Contrast from medial and lateral muscle head groups can be seen in in lower left and right regions of the grid, respectively. THbMb = total-hemo/myoglobin, DOSI = diffuse optical spectroscopic imaging.

Prior to analysis, a medial region of interest (ROI) from the DOSI grid was selected. Medial ROIs were determined using a thresholding criterion that has been used previously to identify and track tumors in breast cancer [30]. Instead of using the tissue optical index, however, we defined a THbMb threshold as

$$\text{threshold}_{\text{THbMb}} = \frac{(\text{THbMb}_{\text{max}} - \text{THbMb}_{\text{min}})}{2} + \text{THbMb}_{\text{min}}$$

where $\text{THbMb}_{\text{max}}$ and $\text{THbMb}_{\text{min}}$ were the maximum and minimum THbMb values for a given leg at baseline. After DOSI data was filtered to only include grid points that met the THbMb threshold, data representing the medial ROI was selected manually to correct for shifting of grid locations from baseline to post-training. After accounting for possible grid-shift, 3-5 grid points were selected for each leg at baseline and data from the same grid points were averaged post-training. Thus, DOSI data for the medial head

ROI represents the same tissue area at both time points. Since the medial ROIs were selected based on higher THbMb content, we believe that they more accurately represent the physiology of the medial gastrocnemius muscle and provide enhanced sensitivity to changes that accompany strength training. The medial ROI data was therefore used when determining which DOSI parameters were sensitive to RT changes, while the entire DOSI grid was used when comparing with DXA results in correlation tests.

3.1.2.6) *DOSI Surface Rendering*

The 3D surface geometry of a sample participant was acquired using a Microsoft Kinect TM for Windows V1 (Microsoft, WA, USA) and the Kinect Fusion SDK. The Kinect also acquires an image of the surface which is textured onto the 3D geometry using open source software Point Cloud Library [33]. The textured 3D mesh is rendered and the measurement points are selected. The optical data, measurement locations, and 3D mesh are imported into MATLAB to generate a 3D interpolated topographic map. A similar process was used in our previous studies of weight loss and breast cancer chemotherapy monitoring to create 3D renderings of DOSI data from abdomen and breast tissue [22, 30]. Not all participants were available for scanning with the Kinect system, so the initial 3D surface geometry from a representative volunteer was used to generate 3D surface images with DOSI data from all participants.

3.1.2.7) *Statistical Analysis*

Throughout this study, we employed the Holm-Bonferroni correction when testing multiple hypotheses and our significance level was defined as $\alpha = 0.05$. All statistical tests were performed with R (R Foundation for Statistical Computing, Vienna, Austria.)

Wilcoxon signed-rank tests were performed to test for changes in repeatedly measured parameters. For DXA, we tested for changes in lower leg LM, FM, and LMF and for DOSI we tested for changes in $HbMbO_2$, HbMbR, THbMb, StO_2, water, and lipid.

Pearson product-moment correlation coefficients were calculated for all 6 pairs of DOSI parameters and DXA LMF. Coefficients were calculated separately for parameters measured at Baseline and Post-Training. Since repeated observations were performed on each participant (data was collected for both legs), there was a possibility that repeated observations would enhance the significance of our correlation tests. To address this issue, mean values between the two legs were calculated for DOSI and DXA parameters before correlation tests were performed so only one data point per person is included in correlation tests [34]. This method allows for a more accurate description of correlations between participants when there are repeated measures for each individual participant [34]. It should be emphasized that this process was more conservative than simply treating all legs as independent contributors to the correlation tests.

3.1.3) Results

3.1.3.1) *Participant Demographics and Strength Training*

The cohort of participants involved a combination of 9 male and 6 female participants ranging in age from 18 – 33 years. DXA was performed on all participants (n = 30 legs) with nine legs assigned to LIT (5 female), ten to HIT (2 female), and eleven to LIT+BFR (6 female). Three participants were not able to contribute to the DOSI results due to system malfunction. Thus, the DOSI data is comprised of twelve participants (n = 24 legs) with seven participating in LIT (2 female), nine participating in HIT (2 female), and eight participating in LIT+BFR (4 female). For the three participants with missing DOSI data, strength data was used in the 1RM comparison between training regimens, but these participants are not included when comparing DXA, DOSI, and 1RM results in the correlation tests.

Participants did not experience significant body weight changes over the course of the study, measuring 67.0 ± 2.0 kg at baseline and 66.9 ± 2.1 kg post-training. While all three training regimens resulted in significantly increased 1RM, there was no statistical difference in 1RM gains when comparing regimens. When all regimens were pooled together, the entire cohort showed a significant increase in 1RM with a 62 ± 9 % change over average baseline values of 70.7 ± 4.9 kg (Δ1RM = 41.5 ± 6.2 kg, p = 1.9E-05). All participants experienced 1RM gains in both legs except for one participant whose 1RM did not change in her right leg. Since no statistical difference was detected in 1RM between separate training regimens, we did not break the participants into sub-cohorts for DOSI and DXA analysis. In addition, we did not observe an association between baseline 1RM and the magnitude of 1RM change.

3.1.3.2) *DOSI Images and Surface Rendering*

Recovered DOSI images were generated for all parameters and data was rendered on a 3D surface geometry from a sample participant (Figure 3). Spatial heterogeneities were present in all images and likely reveal the location of the medial and lateral heads of the gastrocnemius. The images demonstrate changes that take place between baseline (Figures 3A and 3B) and post-training (Figures 3E and 3F) and show that specific regions of the gastrocnemius present greater changes than elsewhere. For the participant's data shown in these images, absorption and reduced scattering coefficients were in the range of 0.010-0.055 mm^{-1} and 0.4-0.8 mm^{-1}, respectively, depending on measurement position and wavelength (Figure 3C, 3D, 3G, 3H). The large range in optical properties was expected as each participant was scanned over a total area of ~220 cm^2.

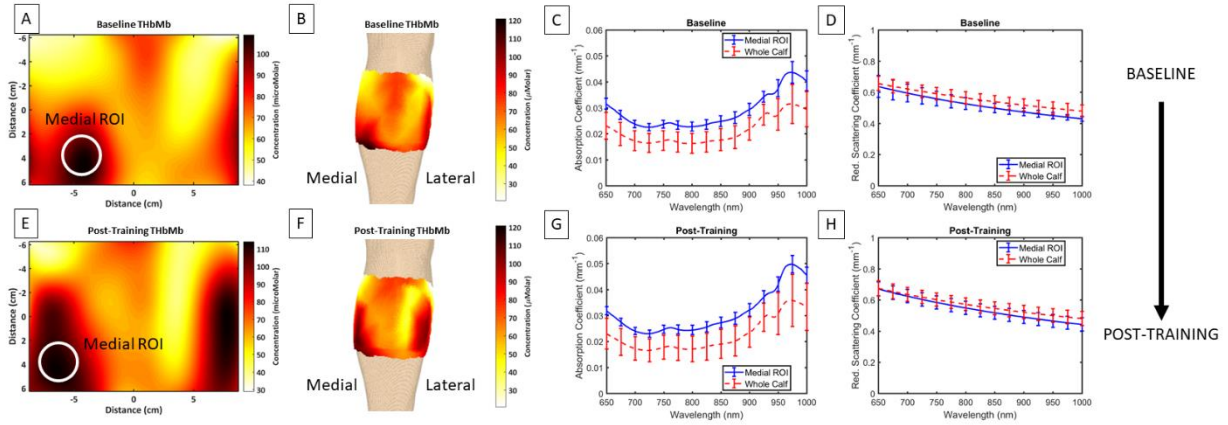

Figure 3. This figure shows sample THbMb DOSI images, THbMb surface renderings, and optical properties for a participant's right leg. A) Baseline DOSI THbMb map with the approximate medial ROI marked. B) Baseline DOSI THbMb surface rendering. C) Mean (±stdev) absorption coefficients across the medial ROI and across the entire calf. D) Mean (±stdev) reduced scattering coefficients across the medial ROI and across the entire calf. E, F, G, H) The corresponding figures 5-weeks post-training. Color bars show concentration of THbMb in microMolar. THbMb = total-hemo+myoglobin, DOSI = diffuse optical spectroscopic imaging.

3.1.3.3) *Correlation Tests*

At Baseline, significant correlations were found between several DOSI parameters and DXA-derived lean mass fraction (LMF) (Table 1, Figure 4). LMF was

positively correlated with $HbMbO_2$ (p = 2.0E-04, R = 0.87), HbMbR (p = 1.2E-03, R = 0.82), Water (p = 1.4E-05, R = 0.93), and THbMb (p = 2.1E-04, R = 0.87) and negatively correlated with Lipid (p = 1.6E-05, R = -0.93).

After training, the same correlations were found between DOSI parameters and LMF (Table 1, Figure 4). LMF was positively correlated with $HbMbO_2$ (p = 8.7E-05, R = 0.89), HbMbR (p = 0.0027, R = 0.78), Water (p = 4.2E-06, R = 0.94), and THbMb (p = 0.0002, R = 0.87) and negatively correlated with Lipid (p = 0.0035, R = -0.77).

Table 1. Pearson product-moment correlation test results between DOSI parameters and LMF from DXA. The Bland-Altman method was utilized in averaging data from both legs of patients to remove the effect of repeated measures. In addition, the Holm-Bonferroni correction was applied to correct for multiple hypothesis testing. Significant correlations are bolded and marked with an asterisk. LMF = lean mass fraction, $HbMbO_2$ = oxy-hemo/myoglobin, HbMbR = deoxy-hemo/myoglobin, THbMb = total-hemo/myoglobin, StO_2 = tissue HbMb saturation, DXA = dual-energy x-ray absorptiometry, DOSI = diffuse optical spectroscopic imaging.

	Baseline		Post-Training	
	R	*p*	R	*P*
$HbMbO_2$	**0.87**	**2.0E-04***	**0.89**	**8.7E-05***
HbMbR	**0.82**	**0.001***	**0.78**	**0.0027***
THbMb	**0.87**	**2.1E-04***	**0.87**	**0.0002***
StO_2	0.61	0.034	0.65	0.0216
Water	**0.93**	**1.4E-05***	**0.94**	**4.2E-06***
Lipid	**-0.93**	**1.6E-05***	**-0.77**	**0.0035***

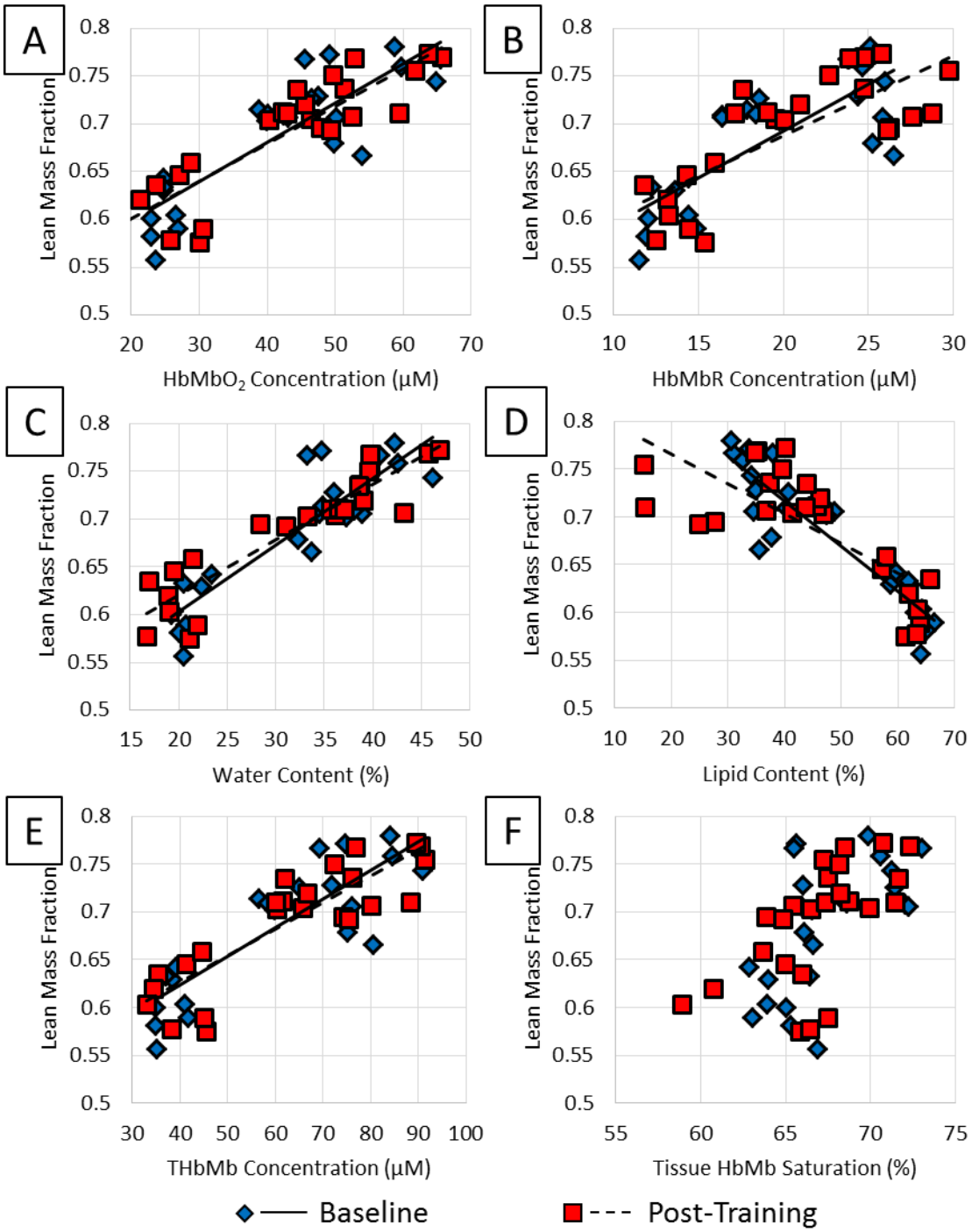

Figure 4. These plots show DOSI parameters plotted against LMF from DXA at baseline and post-training. (A) $HbMbO_2$, (B) HbMbR, (C) Water, (D) Lipid, (E) THbMb, and (F) StO_2. Each data point represents a single leg, so 24 points comprise each plot. Significant correlations were detected between all DOSI parameters shown here and LMF except in (F) where StO_2 vs. LMF did not meet our significance criteria. LMF = lean mass fraction, $HbMbO_2$ = oxy-hemo/myoglobin, HbMbR = deoxy-hemo/myoglobin, THbMb = total-hemo/myoglobin, StO_2 = tissue HbMb saturation, DXA = dual-energy x-ray absorptiometry, DOSI = diffuse optical spectroscopic imaging.

3.1.3.4) *DXA and DOSI Changes with Training*

The only significant DXA change with training was a 2 ± 1 % increase in lean mass (LM) over average baseline values of 2010.7 ± 85.6 g (ΔLM = 36.4 ± 12.4 g, p = 0.01641). Of the 30 legs assessed by DXA, 19 showed gains in LM. After training, DOSI data from the medial region of interest showed significant increases in $HbMbO_2$ and THbMb, with a 6 ± 2 % increase over average baseline values of 57.5 ± 3.5 μM ($\Delta HbMbO_2$ = 3.4 ± 1.0 μM, p = 0.00314) and a 6 ± 1 % increase over average baseline values of 82.6 ± 4.4 μM (ΔTHbMb = 4.9 ± 1.1 μM, p = 0.00024), respectively. Of the 24 legs assessed by DOSI, 18 showed increases in $HbMbO_2$ and 20 showed increases in THbMb. The other DOSI parameters, HbMbR, water, lipid, and StO_2, did not change significantly with training. In all cases, no association was detected between baseline parameters and the magnitude of change after training (Figure 5). In addition, as a secondary set of tests, we evaluated whether the magnitude of DOSI parameter changes were associated with the magnitude of strength change due to training. We did not detect any significant correlations in these secondary tests.

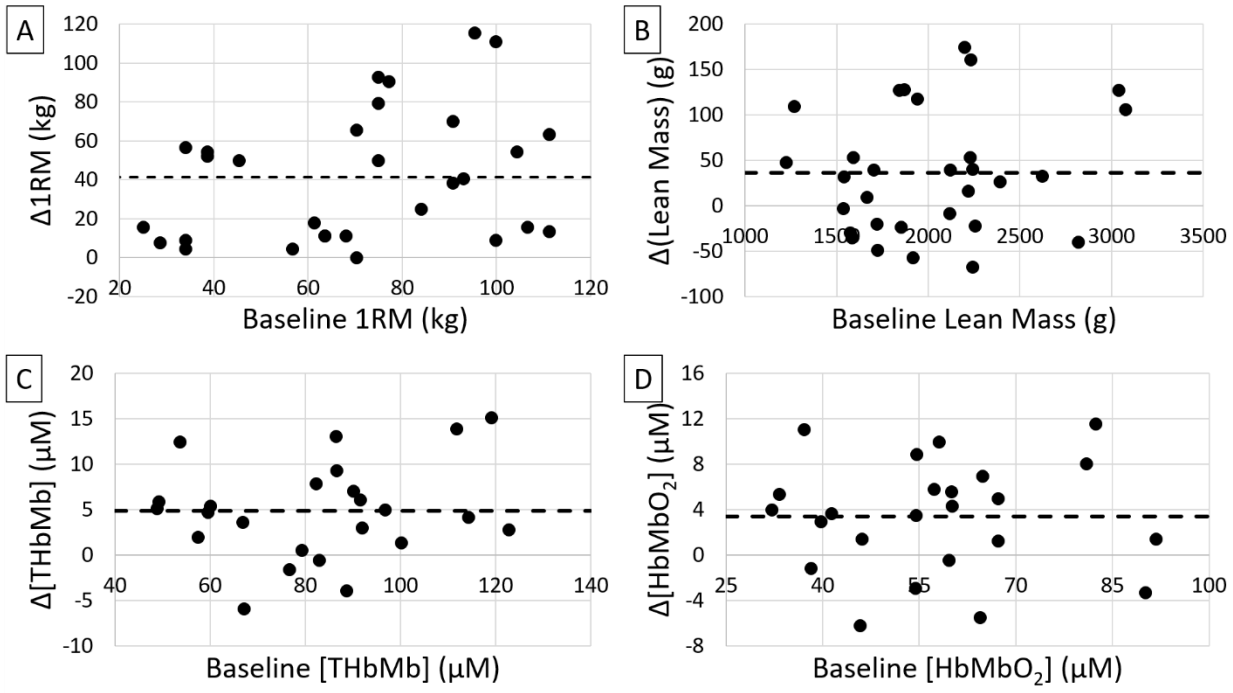

Figure 5. These figures show changes in (A) 1RM, (b) lean mass, (C) [THbMb], and (D) [$HbMbO_2$] that accompanied 5 weeks of resistance training plotted against baseline values. All four parameters showed significant increases (results in text). Each data point represents a single leg from this study, while the dotted line represents the mean change across the entire cohort. The magnitude of change was not associated with baseline values. 1RM = 1-rep-maximum, THbMb = total-hemo/myoglobin, and $HbMbO_2$ = oxy-hemo/myoglobin.

3.1.4) Discussion

NIRS has been widely used in exercise and skeletal muscle research [15-21, 35-41], but there is a lack of research using NIRS to examine how tissue chromophores change during long-term, longitudinal studies as a result of resistance training protocols. To the best of our knowledge, this is the first study to quantify the absolute concentrations of hemo/myoglobin before and after resistance training over a five-week training period. Other researchers have assessed exercise-induced deoxygenation kinetics before and immediately after training [39, 42], but the NIRS techniques used in such studies do not typically quantify light scattering in tissue and are unable to measure absolute levels of chromophore concentrations over an extended period of time. In addition, DOSI used in the present study provides topographic maps of the

change in tissue composition that occurs with resistance training. These assessments reveal spatial variations in the muscle head groups that are used to compare DOSI with DXA, a standard assessment of body-composition.

DOSI images of gastrocnemius muscles appear to differentiate between the superficial lateral and medial gastrocnemius heads. While DOSI is a functional imaging technique, the ability to resolve superficial muscle groups suggests that structural information can be extracted from DOSI. Since a fixed source-detector separation (28 mm) was used in this study, the sampling volume and depth was roughly the same between measurements. This means that locations with thicker subcutaneous adipose layers would have decreased contribution from the underlying muscle. Previous research has shown that an approximate adipose layer thickness can be calculated with NIRS data and it is possible that data from this study could be used in a similar fashion [38]. Future research should examine this concept with the usage of ultrasound imaging or other comparable technology.

Several DOSI parameters reflective of hemoglobin and myoglobin content were shown to linearly correlate with lean mass fraction (LMF) as measured by DXA. This correlation was observed both before and after five weeks of training. While most DOSI parameters were significantly correlated with LMF, StO_2 did not significantly correlate with LMF once the Holm-Bonferroni correction was applied, possibly due to the relatively small sample size. This study suggests that, regarding LMF, DOSI may be equivalent to DXA with no requirement of ionizing radiation. While the imaging performed in this study was limited to the lower leg, DOSI can be used to measure superficial sites throughout the body, and one aim of future work is to determine

whether the correlation between DOSI parameters and LMF is consistent across muscle groups.

Human muscle volume is overwhelmingly composed of myocytes (~80%), with blood vessels comprising a small fraction of muscle volume (~7%) [43]. These proportions emphasize the importance of accounting for myoglobin when describing the chromophore concentrations within muscle tissue. The separation of myoglobin and hemoglobin absorption in muscle tissue is exceedingly difficult because the absorption spectra of the two hemeproteins are very similar. Some groups have reported that it is possible to determine the relative Mb/Hb contributions to NIRS absorption via a combination technique with ^{1}H MRS [40], novel spectroscopic techniques [37], and assumption-based models of human physiology [36, 43]. While early work with NIRS in exercise demonstrated that NIRS deoxygenation signals primarily come from hemoglobin [41, 44], recent work with the above techniques suggests that more than 50% of resting NIRS absorption in muscle is due to myoglobin [36, 37, 40, 43]. These findings are not contradictory but highlight the complex nature of studying muscle with NIRS. If the THbMb concentrations (49 - 123 μM) from this study can be equally attributed to hemoglobin and myoglobin absorption, this suggests that we observed 25 - 62 μM total-hemoglobin and four times as much total-myoglobin, since myoglobin presents only one heme group per protein. It is important to note, however, that non-invasive NIRS measurements of muscle tissue are affected by adipose tissue thickness as well, so our reported values are representative of a bulk, layered tissue structure and not pure muscle tissue.

While significant increases in THbMb and $HbMbO_2$ were seen with training, it is unclear whether these changes come from increased myoglobin content, increased perfusion to formerly closed capillaries before training, increased capillary density, or other modifications throughout the complex skeletal muscle environment. The literature is equivocal on whether myoglobin concentrations in human muscle change with resistance training [45]. Another possibility is that resting blood flow into the gastrocnemius muscles increased and a portion of previously closed capillaries are perfused. Research has shown that resistance training is associated with an increase in the diameter of conduit arteries and peripheral blood flow [46], so this might cause increased perfusion into the downstream arterioles and capillaries. The literature is also inconclusive on whether resistance training affects capillary density, with Tesch et al. reporting a decrease [47], Campos et al. suggesting that it does not change [48], and Hather et al. suggesting that capillary density increases [49]. The number of capillaries per fiber is known to increase with training, however, suggesting that potential increases in capillary density are masked by a concomitant hypertrophic increase in muscle fiber area [48]. If the 5 µM average increase in THbMb witnessed in our study was purely due to changes in capillary density (i.e. no changes in myoglobin concentration or capillary perfusion), this would constitute an 8 - 20% increase over the 25 - 62 µM total-hemoglobin range estimated above. In a sub-group analysis of the study by Campos et al., they noted an 8% decrease for low repetition training (3 – 5 reps), a 4% increase for intermediate repetition training (9 – 11 reps), and a 7% increase for high repetition training (20 – 28 reps) [48]. In addition, they note that the higher repetition training may mimic the characteristics associated with aerobic training, wherein capillary density is

well known to increase. Taking these findings into consideration, the ~6% increase in THbMb seems unlikely to be solely explained by capillary density increases such as those seen in certain training protocols by Campos et al [48]. Given the large (~60%) mean increase in one-rep-max and ~2% mean increase in LM (from DXA) observed in this training protocol, it is likely that several of the above-mentioned mechanisms are contributing to the detected hemeprotein changes. It is also possible that a thinning of the overlying subcutaneous adipose tissue led to a proportional increase in sampled hemo+myoglobin, however this is not supported by corresponding changes in tissue lipid and water content with training.

Tissue lipid and water content were monitored with DOSI but no changes were detected with training. While researchers have suggested that early hypertrophic changes are possibly due to edema from tissue damage, we were unable to verify this with DOSI after five-weeks of resistance training. It is possible that the window to detect edema was missed and participants had adapted to their training by week five. Future studies would benefit from more frequent imaging, particularly in the period immediately after exercise, to measure changes associated with edema.

In summary, we have shown significant correlations between DXA and DOSI information content in the assessment of gastrocnemius muscle composition during a 5-week longitudinal study. These findings suggest that DOSI could be used to assess body composition in a similar fashion to DXA with the advantage of bedside accessibility, frequent measurements, and reduced cost. In addition, we have demonstrated that DOSI is sensitive to changes in concentrations of hemeproteins that accompany resistance training over an extended period of several weeks. This

information could be used to guide training regimens and other long-term interventions designed to improve muscle function, as well as assess and mitigate the effects of muscle wasting and atrophy associated with degeneration and disease. Future studies that include more frequent DOSI measurements and additional imaging correlates could provide further insight into the physiological origins and mechanisms of the spatial and temporal changes in DOSI signals.

3.2) Body Composition: A Pediatric Exercise Study

3.2.1) Introduction to Obesity and Whole-Body Composition Assessment

For at least 30 years, obesity and overweight has become more prevalent throughout the world, with increased prevalence seen in developed and undeveloped countries, in children and adults, and both sexes [50]. Obesity is associated with many additional health issues [51], shortens lifespan [52], and represents excessive personal, industrial, and societal monetary costs [53, 54]. In addition to the need for better prevention and treatment of obesity, enhanced screening and monitoring techniques could play a role in optimizing such prevention and treatment methods. For example, body mass index (BMI) has been used for over 100 years to characterize an individual's body fatness, but it is only an estimate of adiposity. Direct methods to assess body composition involve cadaver analysis, but indirect methods, such as hydrodensitometry or dual energy x-ray absorptiometry (DXA), have been developed which involve some form of assumption about biological tissues. Unfortunately, these more accurate methods to determine adiposity are typically not portable and cannot be accessed by large portions of the population. In addition to more accurate assessments of adiposity,

methods are also needed which provide additional, orthogonal information content that can characterize the metabolic status of individuals. For example, researchers have shown that cardiopulmonary exercise testing, a common biomarker of fitness, is more readily interpretable when an individual's lean body mass is known [55]. For these purposes, low-cost, portable, and quantitative technologies which can assess both body composition and metabolic status could serve an important role in routine clinical examinations.

In the previous section, we demonstrated a relationship between optical measures of heme protein, water, and fat content with DXA measures of lean soft tissue. This finding provided evidence that diffuse optical spectroscopy (DOS) could be used to non-invasively measure body composition in specific tissue compartments. In addition, we have also used DOS to monitor adipose tissue of obese individuals as they underwent caloric restriction and discovered that absorption and scattering changes track and may elucidate metabolic changes which accompany weight loss. These studies were limited to the gastrocnemius and the abdomen, however, and it is unclear how well DOS can be adapted to characterize the entire body.

In this study, we used DOS and DXA to characterize body composition in ~100 participants aged 7 – 34 years. Using DOS, we quantified hemo+myoglobin, water, fat, and the wavelength dependence of scattering in several locations of the body (gastrocnemius, shin, quadriceps, abdomen, biceps). Using DXA, full body scans were performed and a 3-component model was utilized to quantify fat mass, lean mass, and bone mineral content. We demonstrate correlations between several DOS and DXA parameters and propose a DOS protocol for the prediction of whole body fat and lean

soft tissue percentage. Finally, in a subset of tissue locations in which DOS was performed, ultrasound was also used to measure skin+adipose tissue thickness (SATT) and the relationship to DOS-derived parameters is described.

3.2.2) Methods

Participants and Experimental Design

A total of 113 participants were recruited for the study, with 103 completing all DOS and DXA scanning and 100 completing all DOS, DXA, and ultrasound scanning. All testing took place in the Institute for Clinical and Translational Science (ICTS) at the University of California, Irvine. Participants provided written informed consent before their involvement in the study.

Dual Energy X-Ray Absorptiometry (DXA) Measurements

DXA measurements were performed using a Hologic Discovery A DXA system with Apex 3.3 software (Hologic, Marlborough, MA, USA). Prior to scanning, participants removed all metal objects and laid supine on a padded table. A 3-component model was utilized to quantify fat mass (FM), lean mass (LM), and bone mineral content (BMC) for each participant, and each of these parameters were converted to percentages (fat%, LST%, and BM%) by dividing by total body mass.

Diffuse Optical Spectroscopy (DOS) Measurements

DOS measurements were performed using a previously described instrument (2015 Ganesan). Briefly, 3 intensity-modulated laser diodes (690, 785, and 835 nm)

and an avalanche photodiode are used to perform frequency domain photon migration measurements of tissue. At each wavelength, these measurements allow for determination of absorption and reduced scattering coefficients. If the reduced scattering data from the FDPM measurements is fit to expected scattering behavior in biological tissue (Mie theory), broadband reduced scattering coefficients can be obtained in the form

$$\mu_s'(\lambda) = A \times (\frac{\lambda}{500\ nm})^{-b}$$

where A is the scattering amplitude, b is the scattering power, and the denominator is a scaling factor which has been used in previous work to more easily compare results to other studies [5, 22]. In conjunction, a broadband (650-1000 nm) continuous-wave (CW) diffuse reflectance spectroscopy measurement is performed using a quartz tungsten halogen lamp and a miniature spectrometer. The broadband reduced scattering results can be used as previously described to determine broadband absorption coefficients from the CW reflectance results [8]. These absorption coefficients can be further decomposed into basis near-infrared (NIR) absorbers. The dominant NIR absorbers in biological tissue are oxygenated hemo+myoglobin ($HbMbO_2$), de-oxygenated hemo+myoglobin (HbMbR), water, and lipid.

Twelve anatomical sites were chosen and measured with DOS for each participant (Figure 6). These twelve locations were the short and long heads of the biceps (BS, BL), four locations surrounding the navel on the abdomen (LL, LR, UL, UR), the vastus lateralus (VL), rectus femoris (RF), upper and middle shin (SU, SM), and medial and lateral gastrocnemius (GM, GL). At each location, 3 DOS measurements were performed and chromophore concentrations were later averaged over these

separate measurements. The same source-detector separation was used for FDPM and CW measurements and for all participants and anatomical locations: 28 mm.

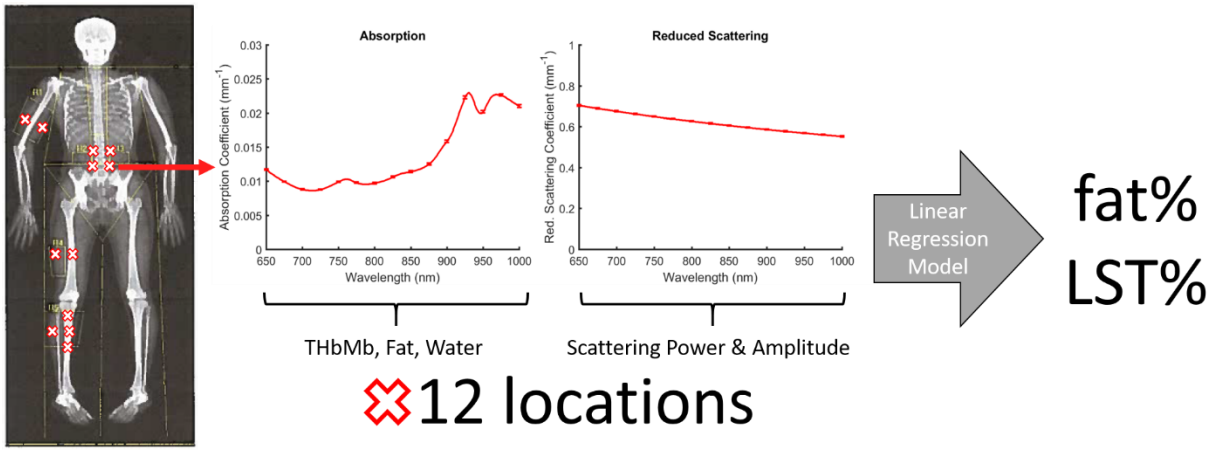

Figure 6. This figure shows how DOS data leads to predictions of DXA fat% and LST%. On the left, a representative DXA image is shown. X marks are placed on approximate locations of DOS measurements. Each DOS measurement contains broadband, 650-1000 nm absorption and reduced scattering coefficients (shown in the middle for an abdominal measurement). These broadband measurements are performed at 12 separate locations and placed into a linear regression model which is fit to DXA fat% and LST% data.

Statistical Analysis

All data analysis and statistical tests were performed within MATLAB (2015a, The MathWorks, Inc.).

Pearson product-moment correlation coefficients were calculated between DXA fat%, LST%, and BM% and all 5 DOS parameters at each of 12 measurement locations (60 tests in total per DXA parameter). This initial set of tests was used to determine if specific parameters of DOS data taken from specific locations explained a significant degree of the variance seen in a corresponding parameter from DXA. If correlations were not significant for a specific parameter at a given measurement location, this DOS data was not considered for our regression model.

Once DOS parameters and locations were selected for regression modeling, participants were randomly assigned to a training subset (n=82) and a test subset (n=21). The training subset was used to build linear regression models while the test subset was used to evaluate the predictive accuracy of the generated models. For regression modeling, data from distinct locations were averaged together such that only one value of each DOS parameter remained for each participant (THbMb, water, fat, scattering power, and scattering amplitude). Finally, the following regression model was used to fit our data:

$$Y_n = \beta_0 + \beta_1(X_{n1}) + \beta_2(X_{n2}) + \beta_3(X_{n3}) + \beta_4(X_{n4}) + \beta_5(X_{n5}) + \varepsilon_n$$

where Y_n is DXA fat percentage for the *n*th participant, β_0 is a fixed effect intercept term, X_{n1}, X_{n2}, X_{n3}, X_{n4}, and X_{n5} represent THbMb, water, fat, scattering power, and scattering amplitude for the *n*th participant, respectively, β_1, β_2, β_3, β_4, and β_5 are regression coefficients for each of the corresponding DOS terms, and ε_n is a random error term which describes all other factors which might influence DXA fat percentage for the *n*th participant.

Finally, while it was important to average data across multiple tissue sites to increase the accuracy of prediction of whole body composition, tissue locations were only used if they added predictive accuracy to the linear model. This selective process was performed by beginning with only one tissue location, that with the strongest individual association with DXA (highest R^2 from training set), in the linear model. After this model was computed, DOS data from the initial tissue location was averaged with a second tissue location and the model was re-calculated. We repeated this process with all possible pairs of tissue locations and the pair with the most accurate prediction

(highest R^2 from training set) was determined. This process was repeated to add a third tissue location to the model, then a fourth, and so on, until the R^2 of the training data no longer increased. In this manner, the combination of tissue locations which comprise the most accurate prediction was eventually identified (Figure 6).

3.2.3) Results

Participant Demographics

In all, 103 participants (54 female, 49 male) aged 7-34 years completed body composition assessments with DOS and DXA. For comparisons between ultrasound skin+adipose tissue thickness (SATT) and DOS on the vastus lateralus and rectus femoris, only 100 of these participants successfully completed DOS and ultrasound assessments.

Optical Properties of Tissues with Respect to Age

While previous studies have described DXA results in similar cohorts to this study [55], optical properties (absorption and scattering coefficients) are still lacking, particularly in younger populations. Optical properties for all 12 anatomical locations can be seen in the appendix of this thesis for participants in early puberty, late puberty, and adulthood (Appendix B). While statistical tests were not performed on these results, there are clear distinctions between certain subcohorts in certain tissues.

Correlation Tests and Regression Model

Significant correlations were detected between most DOS parameters from individual measurement sites and whole body DXA fat% and LST%, with the only exceptions involving scattering amplitude at several measurements sites. Using the initial set of tests as a filter for constructing a regression model, we decided to remove the scattering amplitude predictor term (β_5) from the model and proceed with only four DOS parameters for prediction of fat% and LST%. No associations were detected between DOS parameters and BM% in any tissue sites. For this reason, we did not proceed with model construction for prediction of BM%.

For linear regression modeling, an initial model using only data from one tissue location was generated. All tissue locations were tested at this initial step, but our composite model began with data from the location with the highest R^2 for linear least squares fitting. For both the prediction of fat% and LST%, this tissue location was the short head of the biceps (Figures 7-8). Other tissue locations were added to the linear regression model and root mean square errors for prediction were 2.56% for whole body fat% and 2.50% for whole body LST%, with both models resulting in $R^2 = 0.86$ (Figure 9).

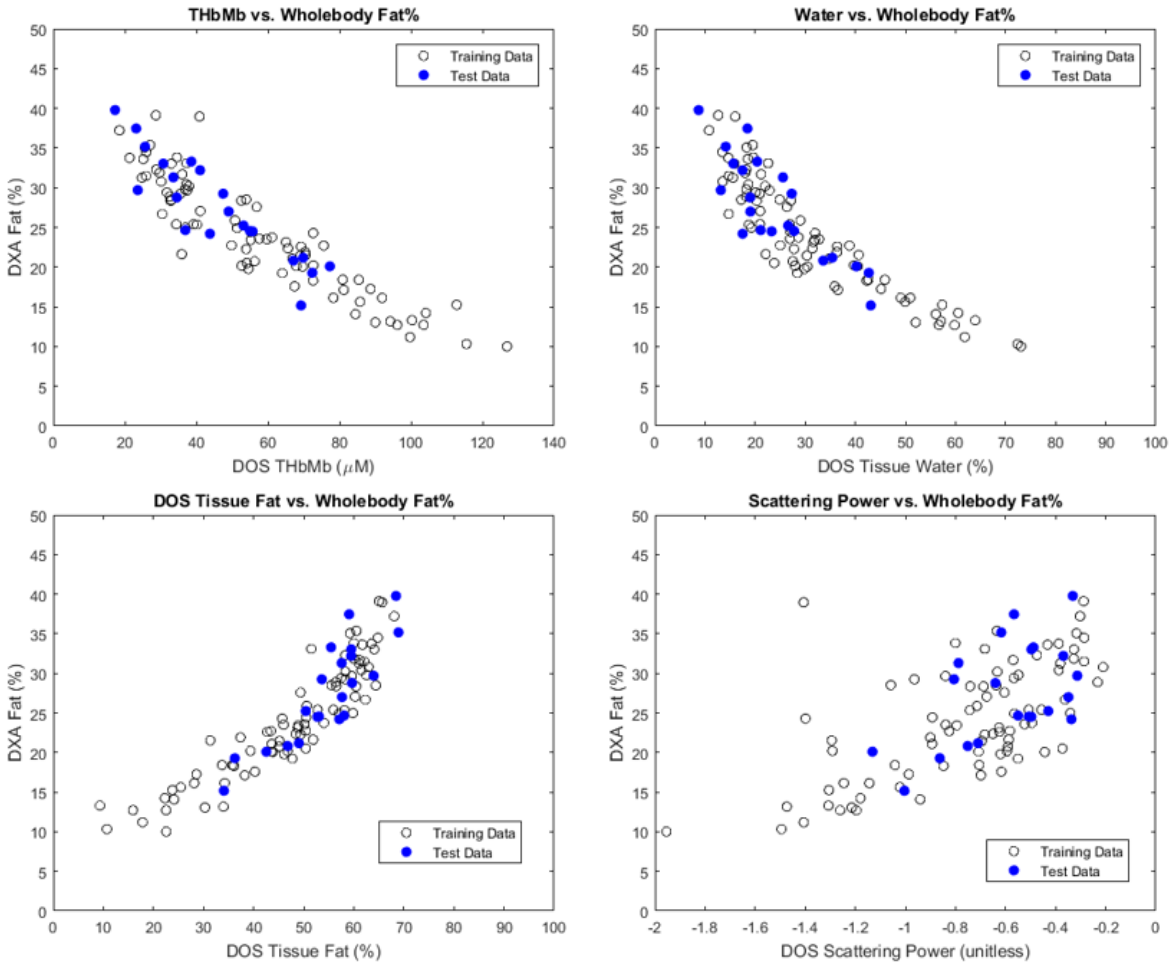

Figure 7. These plots show the relationship between specific DOSI parameters measured from the short head of the biceps (BS) and DXA whole-body fat%. In the upper left and right, negative relationships between DOSI THbMb and fat% and DOSI Water and fat% are seen, respectively. In the lower left and right, positive relationships between DOSI Fat and fat% and DOSI Scattering Power and fat% are seen, respectively.

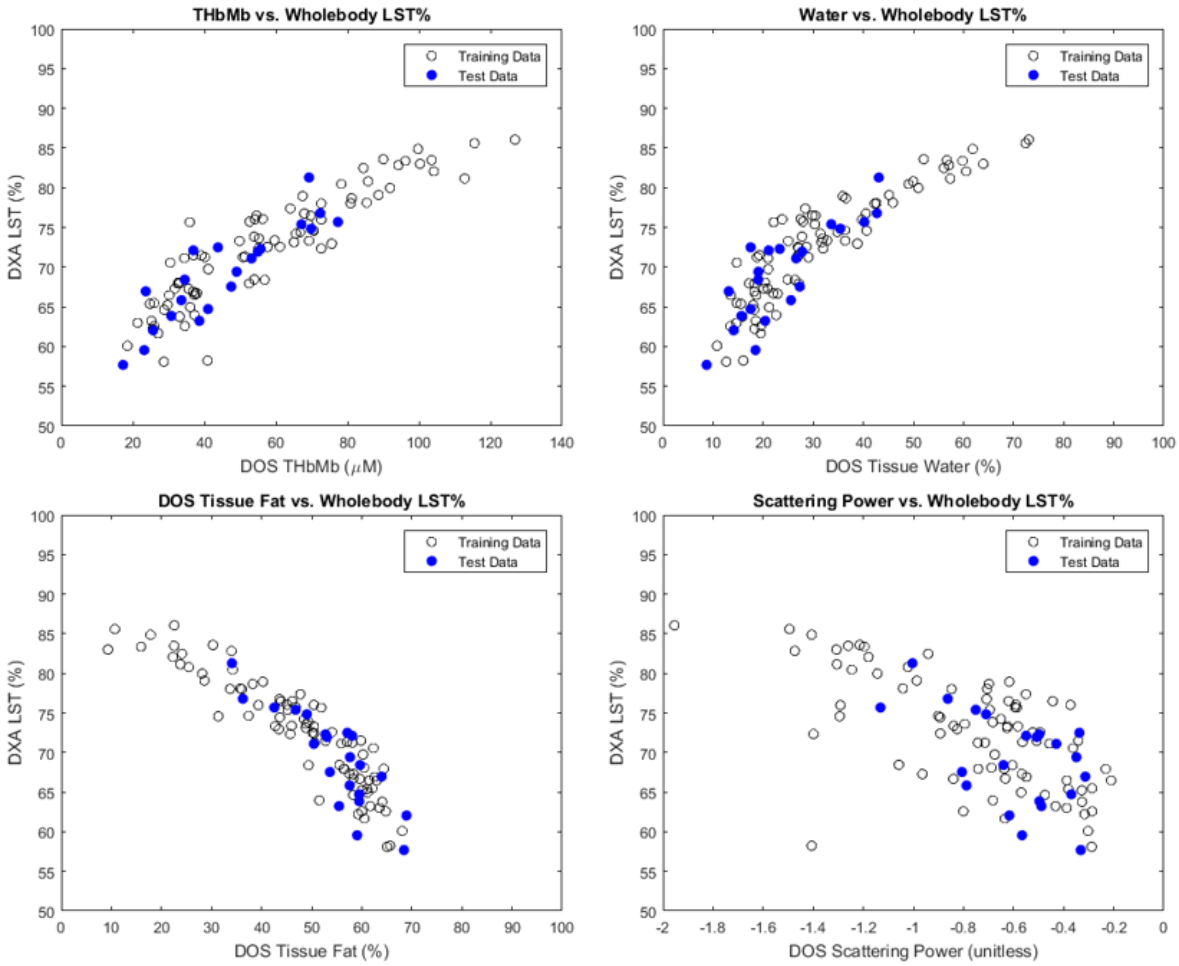

Figure 8. These plots show the relationship between specific DOSI parameters measured from the short head of the biceps (BS) and DXA whole-body LST%. In the upper left and right, positive relationships between DOSI THbMb and LST% and DOSI Water and LST% are seen, respectively. In the lower left and right, negative relationships between DOSI Fat and LST% and DOSI Scattering Power and LST% are seen, respectively.

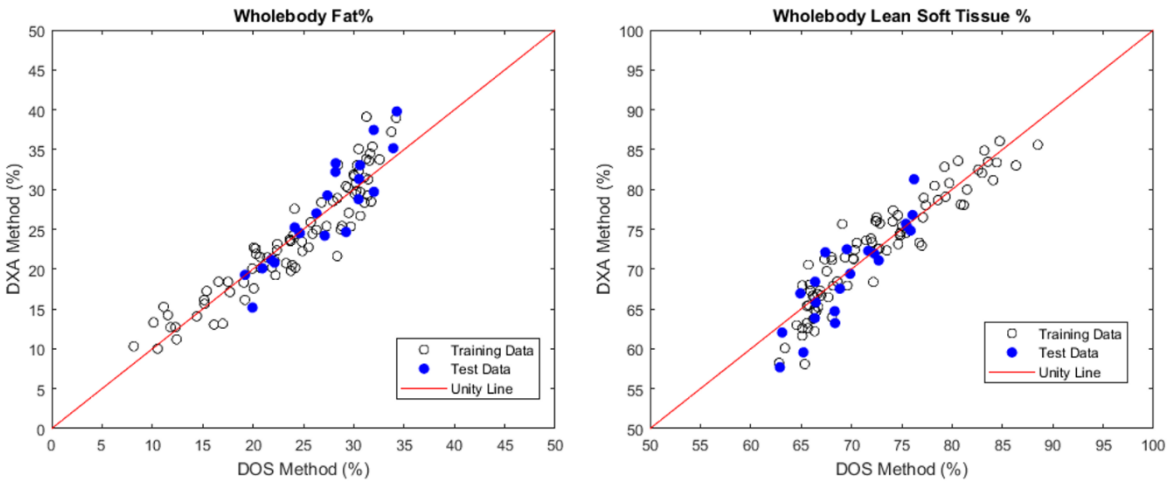

Figure 9. These plots show the final DOSI predictions based on linear regression modeling compared to the actual DXA data. A training data set (white dots) was used to build the linear regression model and a test set was used to evaluate the accuracy of model prediction. Root mean square errors for prediction were 2.56% for whole body fat% and 2.50% for whole body LST%, with both models resulting in R^2 = 0.86. A red line, showing perfect agreement, is shown in each plot.

SATT and DOSI

DOSI results were associated with the skin+adipose tissue thickness (SATT) as quantified by ultrasound. Like the associations described above between DOSI and DXA, the strongest association with SATT was detected in THbMb (Figure 10). SATT ranged from 0.23 – 1.79 cm while THbMb concentration ranged from 15.3 – 152.3 μM. A two-term exponential function of the form

$$THbMb = ae^{b\times SATT} + ce^{d\times SATT}$$

was used to fit ultrasound SATT against DOSI THbMb data (R^2 = 0.87).

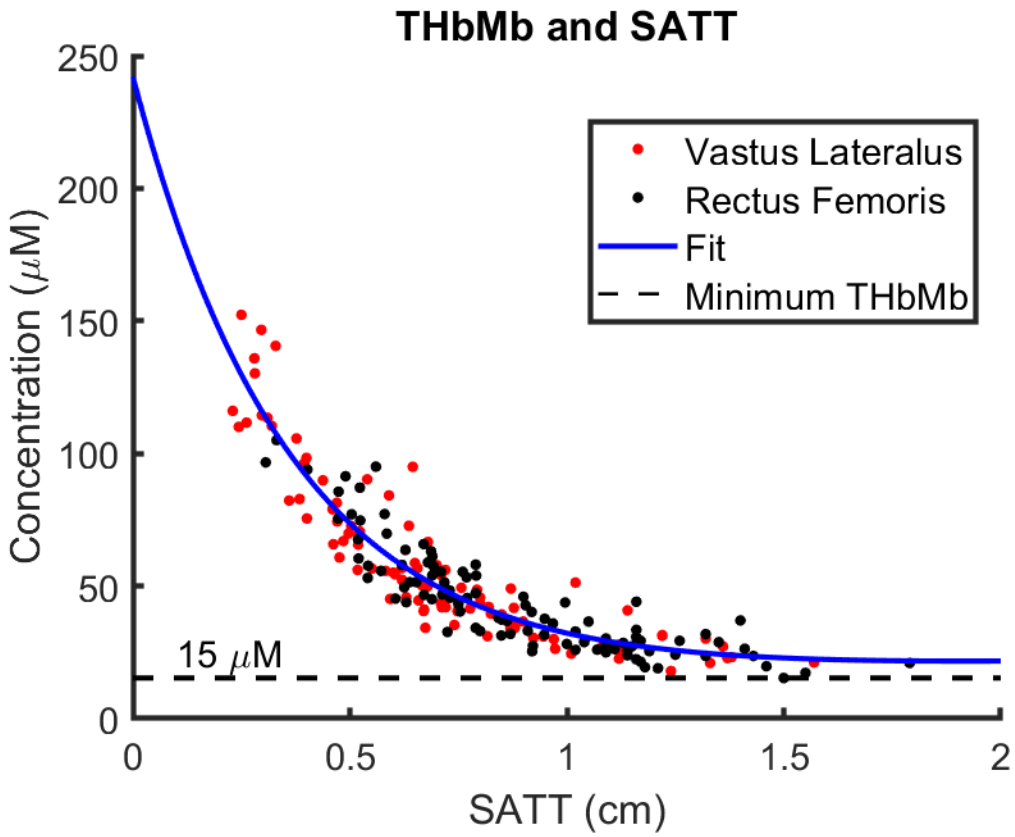

Figure 10. This plot shows the relationship between skin+adipose tissue thickness (SATT) and concentration of THbMb. Data is shown from the rectus femoris and the vastus lateralus. The lowest detected concentration of THbMb was ~15 µM and this is potentially a lower limit where skin and adipose tissue are the primary tissues sampled. A two-term exponential fit is shown in blue and describes the relationship well (R^2 = 0.87).

3.2.4) Discussion

In this study, we show that DOSI can be used to predict whole body fat and lean soft tissue percentages with high accuracy. DOSI information content at a single anatomical location predicts body composition well, but when collected from several locations around the body predictions with minimal error of ~2.5% can be made. This sensitivity is largely due to DOSI's ability to directly sample the thickness of subcutaneous adipose tissue which overlies deeper lean tissues throughout the body.

While many participants (100+) were assessed in this study, most participants were of relatively normal health. Whole body fat percentage ranged from 10 – 40%, with the bulk of participants falling between 15 – 35%. An interesting future study could involve obese individuals or elite athletes which will test the dynamic range of DOSI in each direction. In addition, it is unclear how the presence of disease will affect an individual's results from this type of exam and diseased populations should be carefully studied with age-matched controls.

In this study, optical parameters are highly associated with adipose tissue thickness, but a potential strength of this optical spectroscopic technique is the ability to sense intramuscular fat. While techniques like ultrasound and skin-fold calipers are strictly limited to determining the thickness of subcutaneous adipose tissue for prediction of whole body fat percentage, DOSI takes into consideration the overall composition of a probed tissue volume which will typically contain some amount of muscle. A combination of several factors including disease, obesity, inactivity, age, and injury can lead to a buildup of intramuscular fat [56]. The presence of intramuscular fat can result in dysfunction in metabolism, muscle performance, and mobility [56]. Tools which can assess whole body and specific tissue adiposity have the potential to be impactful in the management of such patients.

Finally, a major result from this study is that high accuracy fat and lean soft tissue prediction with DOSI can be translated into a portable and cost-effective device. While DXA is a powerful technology, its size and cost prevent it from reaching large portions of society. Further minimization and cost-reduction of DOSI is possible and the next section discusses a potential continuous-wave approach based on this study.

3.3) Utilizing Continuous-Wave Data without FDPM

Continuous-wave (CW) Fat-Water Prediction

As described in Chapter 2 of this thesis, the raw continuous-wave (CW) data in DOSI (obtained with a lamp and spectrometer) must effectively be calibrated by the wavelength dependence of scattering which is derived from FDPM. The output of the CW system is a broadband reflectance spectrum which contains information about the overall attenuation due to the medium. However, this attenuation is partially due to light scattering and partially due to absorption. To determine the concentrations of chromophores in a medium, we need the absorption spectrum to be removed from this overall attenuation. FDPM and CW techniques work together to accomplish this goal. A major outcome from this body composition study, however, was a robust characterization of the range of CW responses we obtain when measuring biological tissues. With such a large dataset as a calibration, we attempted to utilize specific features of the raw CW reflectance spectrum to directly obtain chromophore concentrations. Since the wavelength dependence of scattering trends according to an inverse power law, this means the wavelength dependence decreases as wavelength increases. In addition, the relative concentrations of water and fat are often directly in opposition due to tissues being either lean or fatty. With these trends in mind, we hypothesized that CW reflectance within the wavelength range of 900 – 1000 nm could have minimal wavelength dependent influence from scattering and might largely reveal the relative concentrations of water and fat.

Since fat and water have absorption peaks around 930 nm and 970 nm, respectively, we used these two wavelengths to maximize contrast between the two

chromophores. While the output of the CW technique is reflectance as a function of wavelength, it can be converted to a form which is proportional to absorbance by taking a log transform of the inverse of reflectance [57]:

$$"Absorbance(\lambda)" = -log_{10}(Reflectance(\lambda)).$$

Once in this form, we defined a parameter

$$Tissue\ Hydration\ Index\ (THI) = \frac{Absorbance(970\ nm)}{Absorbance(930\ nm) + Absorbance(970\ nm)}$$

which we hypothesized would be associated with the amounts of water and fat in a measured biological tissue. Finally, we used our entire body composition dataset with 12 anatomical locations and 103 participants to fit this THI against typical DOSI-derived concentrations of water (R^2 = 0.90) and fat (R^2 = 0.85) (Figure 11).

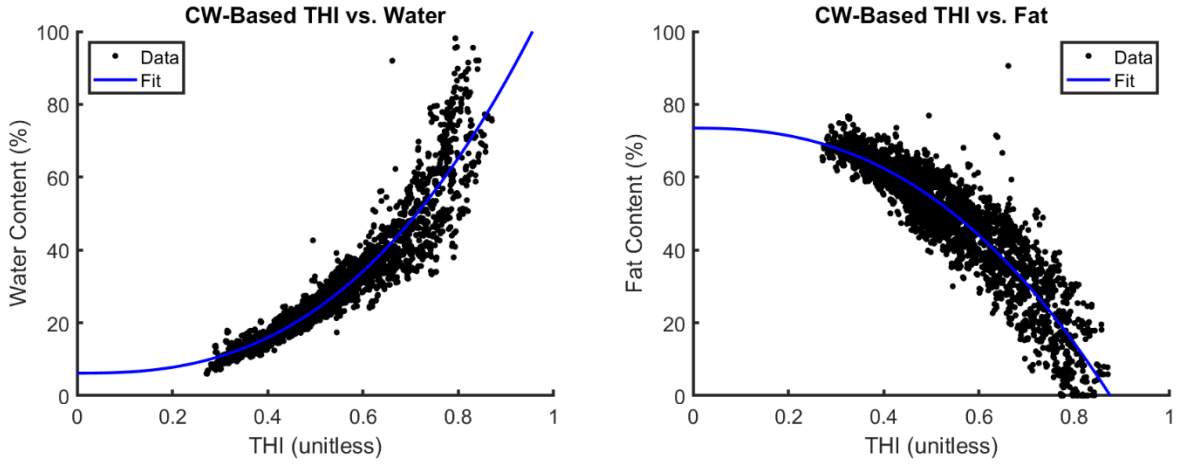

Figure 11. These plots show the relationship between a CW-based metric we term the tissue hydration index (THI) and normal DOSI-derived water and fat content.

These results suggest that a simplified, low-cost approach can be made using only a CW technique to estimate tissue water and fat content. It is possible that these values alone could be sufficient to characterize whole body fat and lean soft tissue percentage.

4) HEMODYNAMIC ASSESSMENT WITH DOS

4.1) Introduction to Vascular Reactivity

Numerous studies have reported endothelial dysfunction to be a strong predictor for adverse cardiovascular events and an underlying feature of PVD. Researchers have discovered that endothelial dysfunction takes place prior to morphological atherosclerotic changes which include inflammation, extracellular matrix digestion, and vascular smooth muscle cell migration and proliferation [58, 59]. These changes in conjunction with endothelial dysfunction act synergistically in a manner that likely leads to atherosclerotic plaque formation [59]. As a result, the vessels begin to stiffen and narrow in diameter, thereby limiting the supply of oxygen to tissue and requiring an increase in cardiac output to compensate.

Arterial stiffness is another important feature of PVD and predictor of cardiovascular risk. Broadly, arterial stiffness describes the structural characteristics of the vasculature such as its distensibility and compliance [60]. The mechanical properties of the vessel walls are dictated by the amount of collagen and elastin present as well as smooth muscle tone [61]. As such, endothelial health also regulates arterial stiffness, mainly by production of NO and other vasodilators. With increased arterial stiffness, the left ventricle of the heart works to maintain output against greater peripheral vascular resistance. This leads to elevations in mean arterial pressure, further PVD, and increased risk of adverse cardiovascular events.

Assessing Vascular Health

Several studies have demonstrated a prognostic role for the assessment of endothelial function [62, 63] and arterial stiffness in CVD [60, 64, 65]. This concept has motivated the development of numerous techniques for assessing these parameters, the most popular of which are coronary epicardial vasoreactivity, ultrasound flow-mediated dilation (US-FMD), venous occlusion plethysmography, and peripheral applanation tonometry. Currently used standard-of-care, non-invasive bedside commercial instruments for assessing endothelial function and arterial stiffness that incorporate these techniques include the EndoPAT (Itamar Medical) and SphygmoCor (AtCor Medical), respectively. In addition, many commercial US devices have features that allow FMD measurements of endothelial function. Although each technology has validated performance features and can be deployed non-invasively at the bedside, one practical limitation is that multiple instruments must be used to determine each characteristic of vascular health. In addition, US-FMD, which is widely considered to be the gold standard for measuring endothelial function, is difficult to perform and highly operator dependent. None of these technologies can provide a complete picture of cardiovascular health by themselves. Combinations of devices can provide a more complete view, but differences in measurement procedures, operator expertise, and equipment costs effectively reduce widespread access. As a result, there is a significant unmet need to develop a single, non-invasive bedside technology that can characterize multiple facets of cardiovascular health in a time- and cost-effective manner. This could provide health practitioners and patients with new opportunities to develop personalized approaches for detecting, managing, and optimizing PVD as well as overall cardiovascular health.

Optical Methods of Monitoring Hemodynamics

There have been many studies demonstrating the potential impact of optical measurements of microvascular hemodynamics [66-70]. De Blasi et al. provided the earliest demonstration of muscle oxygen consumption assessment with near-infrared spectroscopy (NIRS) [66]. NIRS can non-invasively measure the absorbance of chromophores such as oxygenated and deoxygenated hemoglobin to quantify their concentration. The number of distinct chromophore concentrations that can be measured is dependent on the number of wavelengths used. Additionally, NIRS can acquire information at tissue depths on the order of centimeters. Hamaoka et al. further validated oxygen consumption rates measured with NIRS by comparing to ^{31}P-magnetic resonance spectroscopy [67]. In addition to oxygen consumption measurements, vasodilation accompanies changes in blood flow and researchers often use NIRS to study endothelial function [68-70]. There have been studies suggesting that a NIRS assessment of vascular reactivity can also have impact in sepsis [69], peripheral vascular disease [68], and coronary artery disease [70]. These studies all utilize either exercise, injection of vasodilator agents, or induced ischemia to modulate microvascular oxygenation and blood flow. In addition, these studies have demonstrated that NIRS can reliably assess hemodynamics and can be a valuable diagnostic adjunct.

Diffuse Optical Spectroscopic Imaging of a Vascular Occlusion

We have been developing a type of quantitative NIRS technology based on principles of diffuse optical spectroscopic imaging (DOSI) for more than 20 years [71]. Unlike

conventional NIRS, DOSI utilizes hundreds of optical wavelengths (650 - 1000 nm) and broadband, temporally-modulated lasers (50-500 MHz) to quantitatively determine tissue composition (oxy- and deoxy- hemoglobin, water, and lipid concentration) as well as tissue scattering. Calculation of the contribution of lipid and water to the optical signal enables a more accurate determination of the concentration oxy and deoxyhemoglobin. DOSI probes cm-depths into tissue and can quantitatively measure several features relevant to PVD, including tissue composition, vascular reactivity (VR), and the tissue metabolic rate of oxygen consumption ($TMRO_2$) [72].

We have recently begun preliminary DOSI assessments of individuals during vascular occlusion tests (Figure 12). In these tests, baseline measurements are performed for several minutes after which a blood pressure cuff is inflated to a suprasystolic pressure (220 mmHg) for 5 minutes. Following the 5 minutes of blood flow occlusion, the pressure is released and normal blood flow is restored to the tissue. DOSI data is analyzed to calculate absorption and scattering properties of biological tissue throughout the test. Absorption spectra are further analyzed to determine absolute concentrations of oxyhemoglobin (HbO_2) and deoxyhemoglobin (Hb). The result is a continuous assessment of hemodynamics reflective of tissue composition, metabolism, and vascular reactivity (Figure 12).

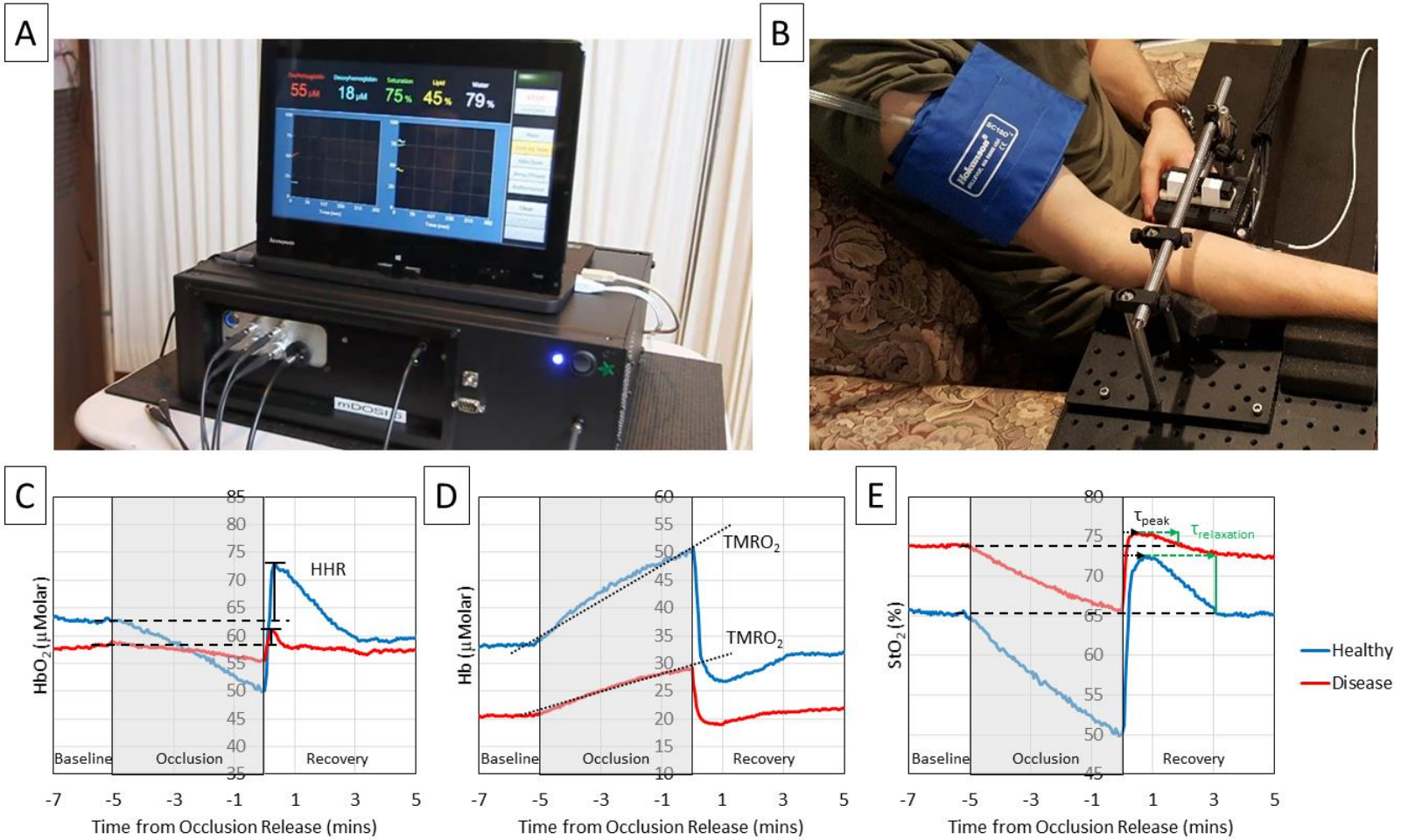

Figure 12. (A) A DOSI device. (B) A study participant during a vascular occlusion test. (C, D, & E) HbO_2, Hb, and StO_2 are shown for a healthy control and a patient with known endothelial dysfunction. Each graph shows baseline (2 minutes), occlusion (5 minutes), and recovery (5 minutes). In these hemodynamic results, resting tissue composition can be determined during the baseline phase. The occlusion phase allows for calculation of the tissue metabolic rate of oxygen consumption ($TMRO_2$). The recovery phase allows for calculation of a hemodynamic hyperemic response (HHR) as well as time-dependent parameters representing the vasculature's adaptation to increased blood flow (τ_{peak}) and the slower relaxation ($\tau_{relaxation}$) back to baseline.

In a vascular occlusion test, we calculate several parameters with DOSI (Figure 12). Tissue composition is determined during the baseline of the test in terms of HbO_2 and Hb concentrations. During the occlusion phase, the tissue metabolic rate of oxygen consumption ($TMRO_2$) is determined by calculating the rate of change of Hb. Finally, the recovery phase allows for quantification of hemodynamic hyperemic response (HHR), the time-to-peak (τ_{peak}) following occlusion release, and the time for relaxation back to baseline ($\tau_{relaxation}$). The HHR is defined as the percentage increase from baseline HbO_2 to post-occlusive peak HbO_2. The τ_{peak} is the time required following occlusion release to reach peak StO_2 and $\tau_{relaxation}$ is the time required to relax from peak StO_2 back to baseline StO_2. While additional parameters can be calculated from this rich data set, these specific parameters have been identified because of: (a) unique advances over previous near-infrared spectroscopy (NIRS) work, (b) correspondence to previous NIRS work, and (c) correspondence to EndoPAT and Ultrasound-FMD outcomes.

4.2) Metabolism and Vascular Reactivity in Healthy Controls

4.2.1) Methods

Participants and experimental design

A total of 13 participants (5 female, 8 male) were recruited for this study. Participants were limited to non-smokers, those without known cardiovascular diseases, and people between the ages of 18 – 40 years old. The study took place at the Beckman Laser Institute and Medical Clinic, University of California, Irvine, and the study protocol was approved by the Institutional Review Board of University of California, Irvine.

Participants were asked to avoid alcohol, caffeine, and exercise on the day of their study visit and provided written informed consent prior to all assessments.

Study Protocol

Participants sat in a relaxed position for at least 15 minutes prior to the collection of optical data to ensure a stable baseline. During this time, an automated blood pressure cuff (Hokanson, Inc., Bellevue, WA, USA) was placed around the upper right arm and optical probes were placed distal to the cuff on the right arm (Figure 12). Baseline optical measurements were acquired for 5 minutes prior to inflation of the blood pressure cuff to 220 mmHg which established an arterial/venous occlusion. The vascular occlusion was released after 5 minutes and 10 minutes of recovery data was collected. After the full 20 minutes of optical data was collected, blood pressure, height, and weight were measured. Finally, ultrasound was used to measure the adipose tissue thickness where the DOSI probe had previously been placed.

Diffuse Optical Spectroscopy

Diffuse optical spectroscopic imaging (DOSI) has been described in detail previously [73] but a brief overview will be provided here. DOSI combines frequency domain photon migration (FDPM) and continuous-wave, broadband spectroscopy to obtain absorption coefficients ($\mu_a(\lambda)$) and reduced scattering coefficients ($\mu_s'(\lambda)$) across a broad range of wavelengths (650 – 1000 nm). For FDPM, three intensity-modulated laser diodes (690 nm, 785 nm, and 830 nm) were used for illumination and an avalanche photodiode detector was used to collect the diffusely reflected light in the form of photon

density waves. For broadband spectroscopy, a quartz tungsten halogen lamp was used for illumination and a spectrometer was used for light detection. The two methods were combined into a single probe and interrogated approximately the same tissue volume with source-detector separations of 22 mm. The resulting broadband absorption coefficients allow for an absolute calculation of chromophore concentrations in bulk tissue. The primary chromophores contributing to absorption and recovered in this study are oxy-hemo+myoglobin ($HbMbO_2$), deoxy-hemo+myoglobin (HbMb), water, fat, and the derived parameters total-hemo+myoglobin (THbMb = $HbMbO_2$+HbMb) and oxygen saturation (StO_2 = $HbMbO_2$/THbMb). DOSI measurements were performed approximately every 15 seconds throughout the 20-minute test session.

Diffuse Correlation Spectroscopy

A diffuse correlation spectroscopy (DCS) device was also used in this study to quantify blood flow during the vascular occlusion test. The device has been described previously [74] but will be briefly described here. A long coherence length 785 nm laser was coupled into a 200 μm optical fiber and placed alongside DOSI fiber sources in a larger probe housing. Two single mode fibers were used for DCS collection and these were placed near the DOSI detectors so a comparable tissue volume was studied. After collection of remitted light into these optical fibers, light was transmitted to two photon-counting modules. The outputs of these detectors were connected to a hardware correlator board to measure the auto-correlation function of the detected signal. This autocorrelation function is sufficient to quantify movement of particles in the

studied medium and in the case of these experiments it allows for quantification of blood flow.

Diffuse Reflectance Spectroscopy and Laser Doppler Flowmetry

In addition to DOSI and DCS, skin microcirculation was measured using a PeriFlux 6000 EPOS system (Enhanced Perfusion and Oxygen Saturation; Perimed AB, Järfälla, Stockholm, Sweden), integrating diffuse reflectance spectroscopy (DRS) and laser Doppler Flowmetry (LDF) in a fiber-optic probe. The system consisted of a PF 6010 laser Doppler unit, a PF 6060 spectroscopy unit, a broadband white light source (Avalight-HAL-S, Avantes BV, the Netherlands) and a fiber-optic thermostatic heating probe. The PF 6010 unit contains a laser light source at 785 nm and a thermostatic heating controller. The PF 6060 unit had two spectrometers (AvaSpec-ULS2048L, Avantes BV) and an optical notch filter behind the slit in the spectrometers to ensure minimal influence from the PF 6010 laser light source on the DRS spectra by suppressing wavelengths 790±20 nm. The fiber-optic probe (Figure 13), consisted of two central emitting fibers and three detecting fibers. The fiber for the LDF laser light source and the LDF detecting fiber at a distance of 0.8 mm had a core diameter of 125 µm. Two detecting fibers were placed at distances of 0.4 and 1.2 mm from the fiber connected to the white light source and were connected to one spectrometer each. Those fibers had a core diameter of 200 µm and all fibers had a numerical aperture of 0.37 and were made of fused silica. During the measurements, the probe was fixated to the skin using rings of double-sided adhesive tape (PF 105-1, Perimed AB), not covering the fiber ends.

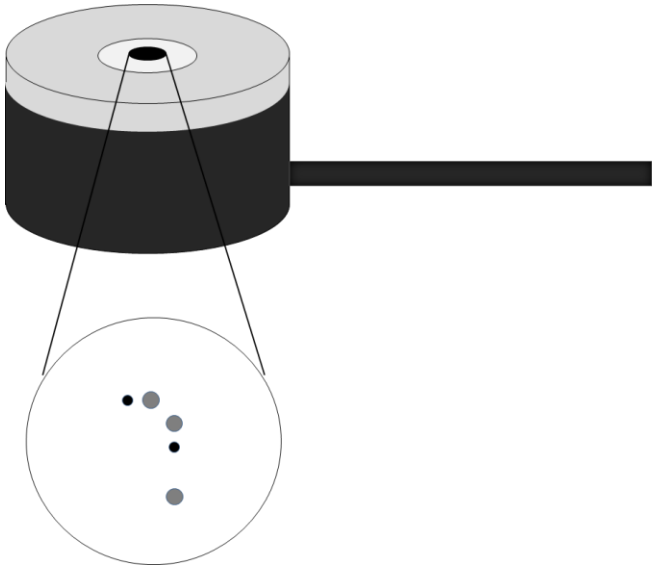

Figure 13. Fiber optic probe with fiber configuration. The probe (D = 23 mm), included a thermostatic heater, a central black part with fibers (D = 3 mm), a central white ring where adhesive tape is not attached to and the outer light grey ring where the double adhesive tape is applied. The fibers are two LDF fibers (black; D = 125 µm) and three DRS fibers (grey; D = 200 µm). The upper two fibers are the LDF and DRS source fibers. DRS detector fibers are at distances 0.4 mm and 1.2 mm from the source, while the LDF detector fiber is at 0.8 mm from the source.

Data Analysis and Statistics

Several parameters were quantified using the optical techniques. During the baseline portion of the vascular occlusion test, blood flow, total hemoglobin concentrations, and tissue oxygen saturation were quantified from DOSI and DCS. During the occlusion portion of the test, the tissue metabolic rate of oxygen consumption (TMRO2) was determined by performing a linear fit to the deoxyhemoglobin concentrations over time. TMRO2 was determined in deep tissue and skin. For the deep tissue technique, 2 minutes of data was used for the fit while in the skin technique 15 seconds was used. In our occlusion experiment, we directly

measure the rate of change of deoxygenated hemoglobin, $\frac{\Delta Hb}{\Delta t}$, in units of μMolar per minute. Since there are four molecules of oxygen bound to each hemoglobin complex, the rate of oxygen consumption is 4 times this value, or

$$\Delta O_2 = (4 \cdot \Delta Hb)\ \mu Molar \cdot min^{-1}, or\ \mu mol \cdot L^{-1} \cdot min^{-1}.$$

If we make certain assumptions about the environment in which oxygen is located, namely the specific gravity of tissue, temperature, and pressure, then we can convert to more popularly published units of oxygen consumption. First, we assume that tissue has a specific gravity of 1.06 kg/L,

$$\Delta O_2 = (4 \cdot \Delta Hb)\ \mu mol \cdot \frac{1}{L} \cdot \frac{1\ L}{1060\ g} \cdot min^{-1}.$$

Finally, we assume that the volume of 1 mole of O2 gas is 22.4 liters at standard temperature and pressure,

$$\Delta O_2 = \frac{22.4 \cdot (4 \cdot \Delta Hb)}{10.6}\ \mu L \cdot (100\ g)^{-1} \cdot min^{-1} = \ (0.008 \cdot \Delta Hb)\ ml \cdot (100\ g)^{-1} \cdot min^{-1}.$$

During the recovery portion of the test, hyperemic responses in oxyhemoglobin concentrations and blood flow were quantified for deep tissue and are reported as a percentage change from baseline. These two results for oxyhemoglobin and blood flow are respectively defined as

$$HbO_2HR = \frac{(HbO_{2_{baseline}} - HbO_{2_{peak}})}{HbO_{2_{baseline}}} \times 100\%$$

and

$$BFHR = \frac{(BF_{baseline} - BF_{peak})}{BF_{baseline}} \times 100\%\ .$$

In addition to quantification of the above parameters, each of the parameters is compared to SATT to demonstrate if and how the parameters are dependent on SATT.

4.2.2) Results

Participant Demographics

All 13 recruited participants completed the study. Age, height, weight, blood pressure, heart rate, and forearm adipose tissue thickness for each participant can be seen in Table 2.

Table 2. Demographic and physical information for participants in this study.

Participant #	Gender	Age (yrs)	Height (cm)	Weight (kg)	Systolic BP (mmHg)	Diastolic BP (mmHg)	HR (bpm)	Adipose Tissue Thickness (cm)
1	F	29	171	62.8	109	92	68	0.68
2	M	29	176	61.9	142	91	76	0.35
3	M	25	175	53.0	110	80	67	0.15
4	M	27	182	73.7	134	96	69	0.26
5	M	23	175	70.5	119	55	71	0.20
6	M	22	192	77.1	136	76	68	0.35
7	F	24	170	65.8	123	78	72	0.55
8	F	21	175	57.7	121	89	96	0.60
9	F	34	173	63.5	99	91	57	0.47
10	M	38	177	78.5	119	87	76	0.48
11	F	25	165	55.3	111	75	71	0.58
12	M	38	180	84.5	130	97	65	0.45
13	M	25	200	83.0	132	87	82	0.30
	AVG	28	178	68.3	122	84	72	0.44
	STDEV	6	9	10.4	13	11	9	0.15

Optical Results

Participants presented a range of occlusion responses with a strong overall dependence on SATT. In general, deep tissue assessments resulted in baseline and dynamic results which were damped in magnitude with thicker SATT (Figures 14A & 14C) compared to thinner SATT (Figures 14B & 14D). At baseline, deep tissue THbMb concentrations showed a significant inverse relationship to SATT (R^2 = 0.9162) (Figure

15A). For deep tissue hemodynamic results, $TMRO_2$ (Figure 15B), HbO_2HR (Figure 15C), and BFHR (Figure 15D) were inversely related with SATT, but only $TMRO_2$ results reached statistical significance (R^2 = 0.5944, 0.3849, and 0.2405 respectively). The only measure that was extracted from the skin assessment technique was TMRO2 and this did not show a significant relationship to SATT (R^2 = 0.26) (Figure 15B).

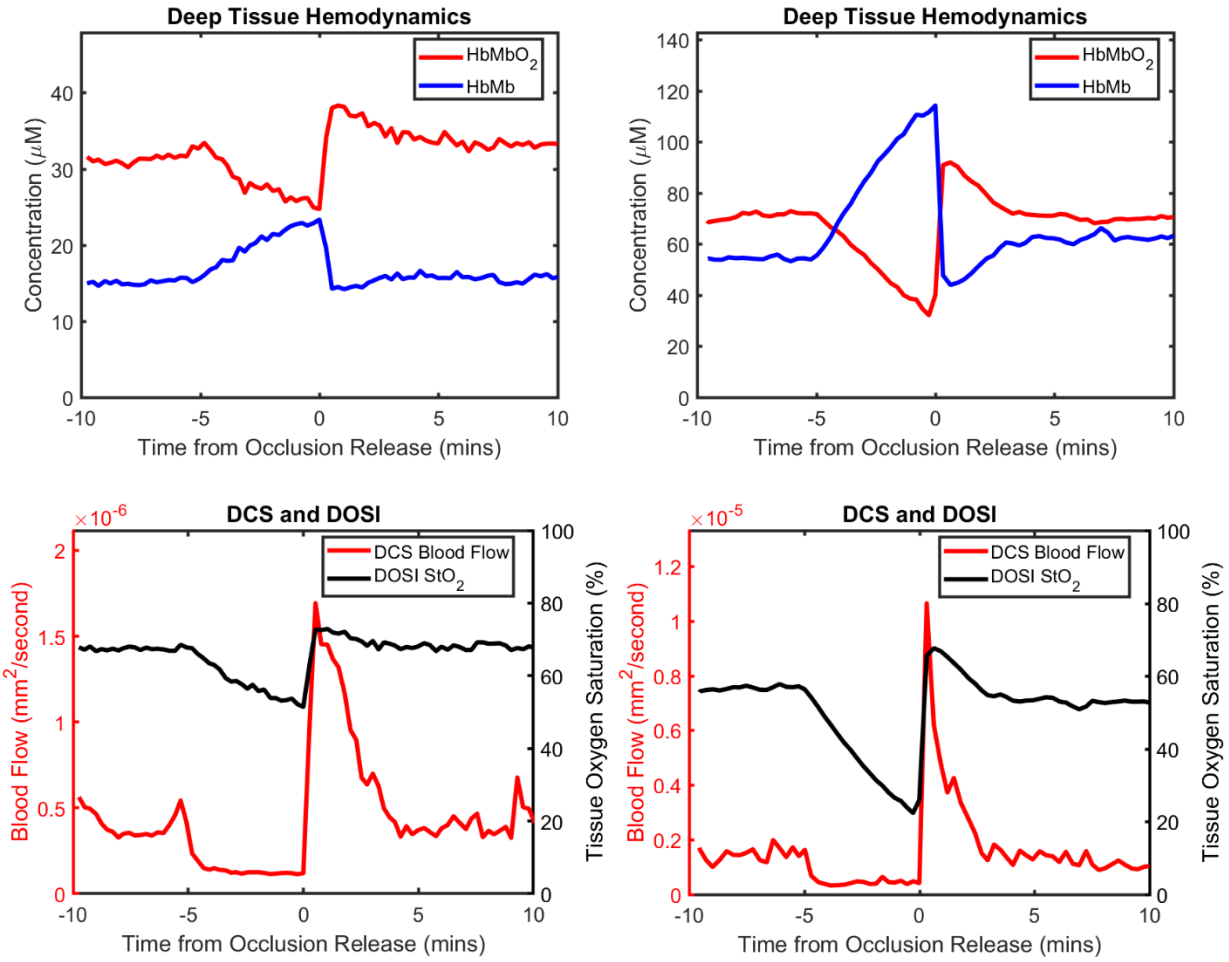

Figure 14. These plots show deep tissue hemodynamic responses from the vascular occlusion test for 0.55 cm (left) and 0.35 cm (right). In the top row, much lower baseline concentrations of $HbMbO_2$ and HbMb are seen in the participant with thicker SATT (15-40 μM vs. 30-120 μM). Damped $TMRO_2$ can also be seen during the occlusion phase of the test in the participant with thicker SATT. In the bottom row, StO_2 and blood flow are displayed for each participant. StO_2 does not drop as low in the participant with thicker SATT, but blood flow levels do not seem dependent on SATT.

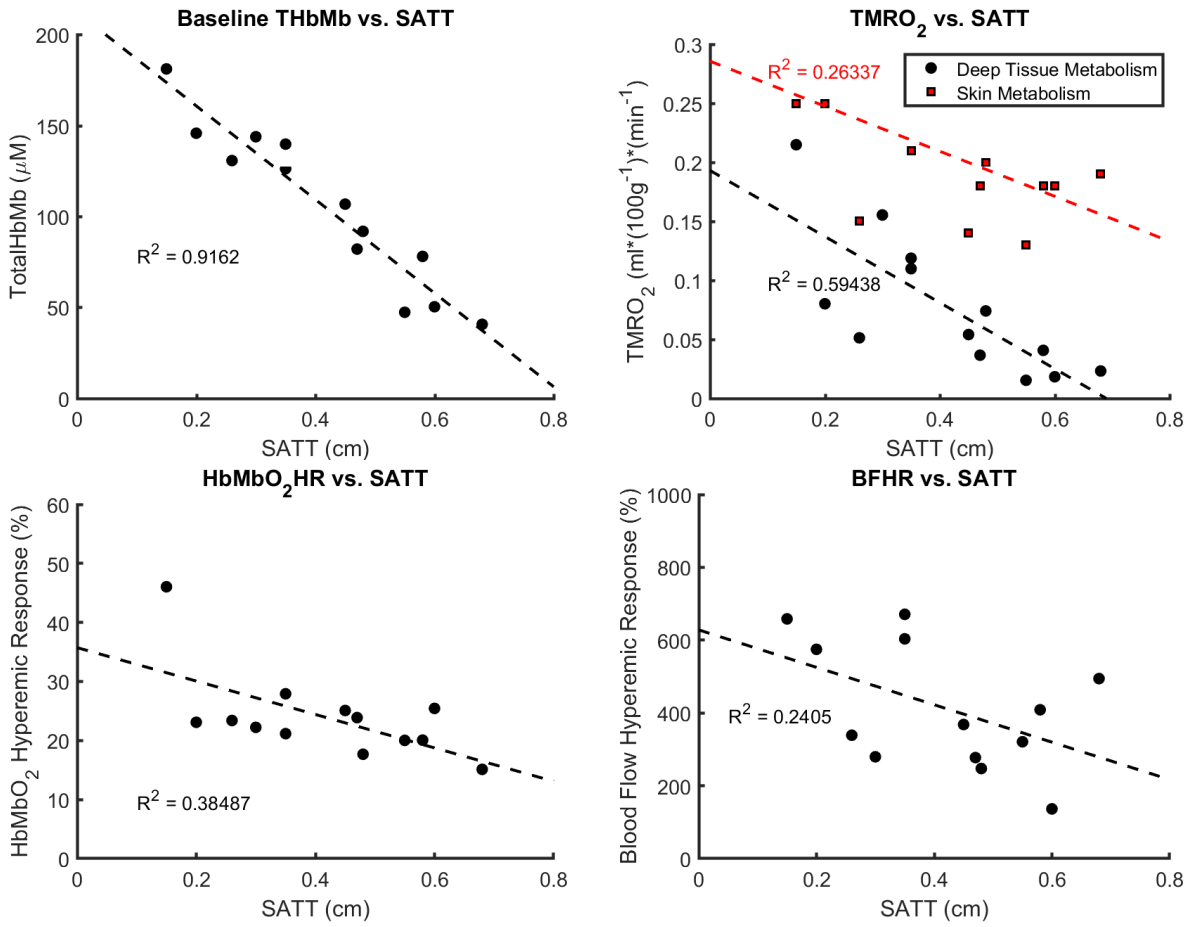

Figure 15. These plots show the relationship between optical parameters and SATT. In the upper left, a significant association is shown between baseline THbMb and SATT. Similarly, in the top right, $TMRO_2$ for the deep tissue technique is significantly associated with SATT. The skin technique's $TMRO_2$ results are also shown in the top right, but the results were not significantly associated with SATT. Similarly, $HbMbO_2HR$ and BFHR are shown against SATT in the bottom plots but no significant associations were detected.

4.2.3) Discussion

In this study, we characterize the range of vascular occlusion results for a healthy population. A major confounding factor in previous studies of hemodynamics has been SATT. In this study, we quantified SATT in all participants and characterize the relationship between SATT and hemodynamic parameters of interest.

As expected, a strong relationship was seen between SATT and deep tissue results. Both baseline composition (THbMb) and metabolic rate ($TMRO_2$) were

significantly associated with SATT. However, hyperemic response parameters in both hemoglobin and blood flow did not seem significantly related to SATT. The range of results for TMRO2 agree with previous reports in literature. Niwayama et al. used a spatially resolved continuous-wave device to study vascular occlusions in 13 healthy males [75]. A similar range of SATT was noted in their participants and TMRO2 ranged from ~0.025 – 0.15 $ml \cdot (100g^{-1}) \cdot (min^{-1})$.

These results demonstrate that DOSI can reliably measure hemodynamic parameters throughout a vascular occlusion test, however, SATT is a major confounding issue and must be addressed. It is possible that multi-layer models could clarify results if multiple source-detector views are utilized. Such a technique would allow for a unique characterization of both adipose and the underlying muscle tissues.

4.3) Using Multiple Source-Detector Views to Account for Adipose Tissue

As demonstrated in the previous section, SATT is a major confounding factor for hemodynamic tests when deep tissue assessment techniques such as DOSI are used. As a follow-up to the previous study, we constructed a two source-detector (10 mm and 20 mm) system in our lab and performed preliminary testing on two individuals with different SATT (3 mm and 6 mm). While this study is in its preliminary stages, it demonstrates how a two source-detector system could help to better characterize vascular occlusion tests.

Both individuals were monitored for two minutes on the inner forearm, approximately the same location used in the previous section. After two minutes of baseline data collection, a blood pressure cuff was inflated to 200 mmHg and was left

inflated for three minutes. Following the three minutes of occlusion, the pressure was released and the individuals were monitored for another three minutes (Figures 16-18).

In Figure 16, the relationship between source-detector separation and composition can be seen. Even with a larger source-detector probe, the individual with 6 mm of SATT shows a resting composition that is largely adipose tissue. In Figure 17, only the occlusion response in deoxyhemoglobin is shown and a linear fit is performed on the data. These results show the magnitude of metabolism change between the overlying SATT and deeper muscle tissue. If we assume that the shorter source-detector probe is largely not sampling the underlying muscle tissue, it seems that resting muscle metabolism is >6x higher than adipose tissue metabolism. Finally, in Figure 18, the hyperemic response of $HbMbO_2$ does not seem related to the individual's SATT. While an increase in source-detector separation resulted in an increased magnitude of hyperemic response, the participant with thicker SATT seems to have a larger hyperemic response than the thinner participant. This result confirms our findings from the study of the previous section that hyperemic response is not significantly related to the overlying SATT. The arterial end of the vasculature contains endothelial cells and will dilate in response to changes in blood flow. Since arteries reside deeper in tissue than veins, it makes sense that the deeper DOSI probe would detect a greater magnitude of hyperemic response.

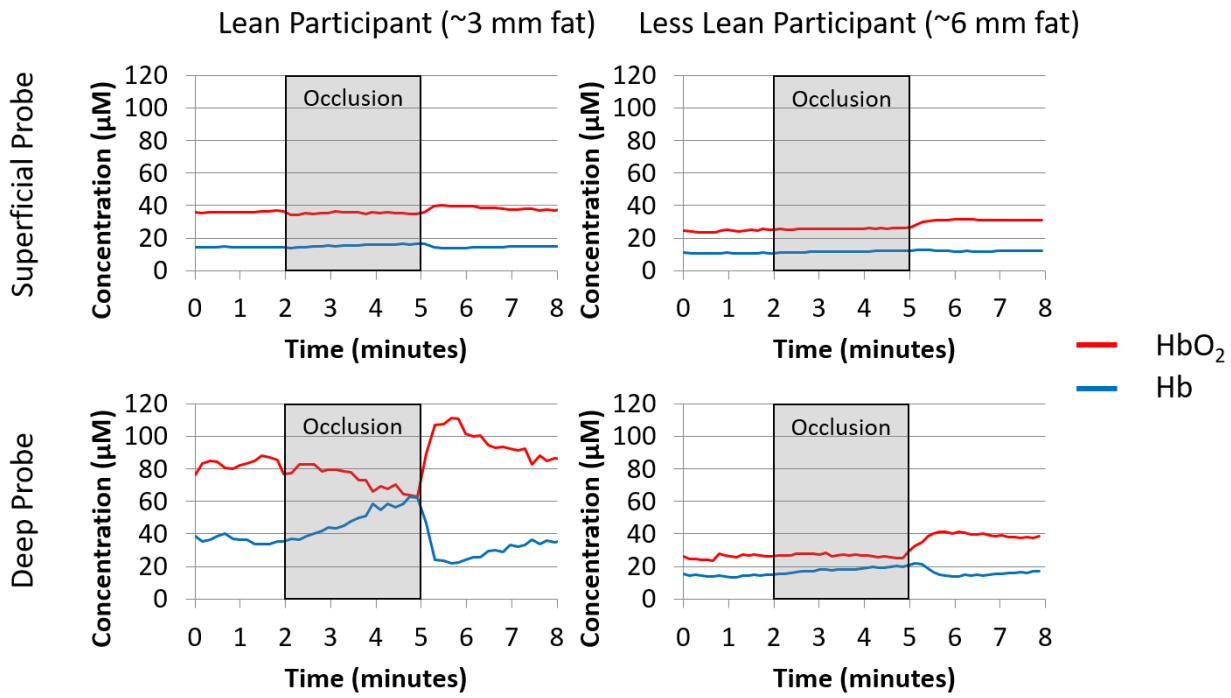

Figure 16. These plots show composition results from vascular occlusion tests for two individuals (left and right) using our two-channel DOSI system. The top row shows results in the two individuals using a superficial probe with a source-detector separation of 10 mm. The bottom row shows results in the two individuals using a deep probe with a source-detector separation of 20 mm. While the deep probe seems to be interrogating muscle in the lean individual (bottom left), the other results seem dominated by adipose tissue.

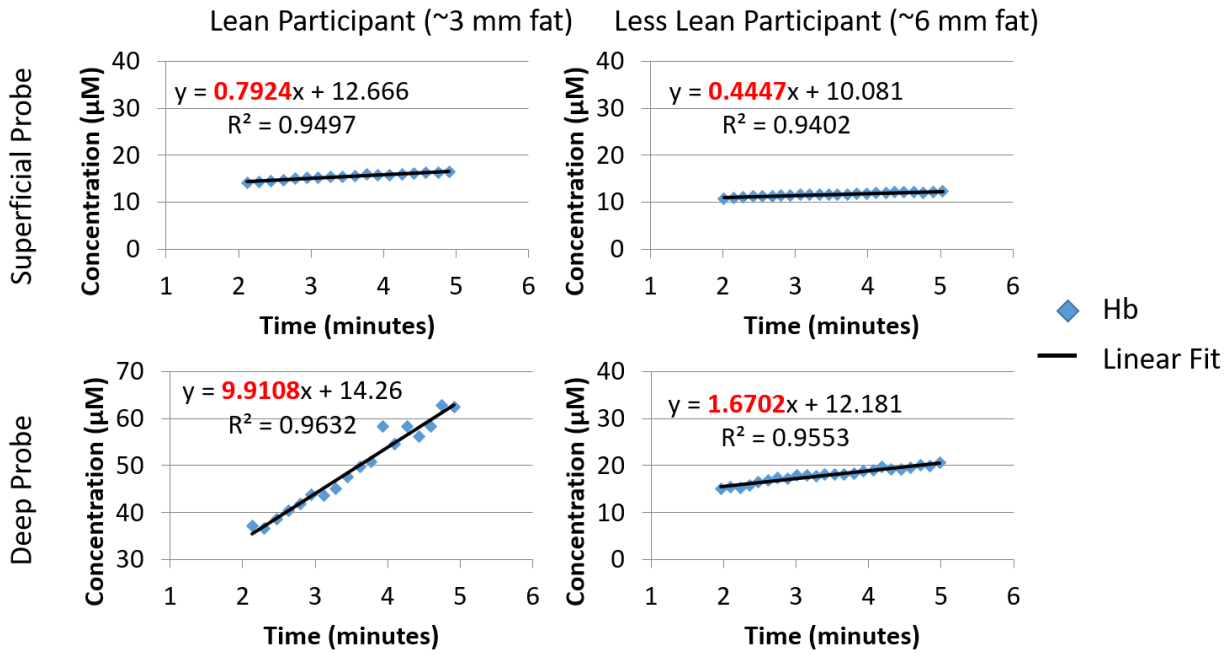

Figure 17. These plots show deoxyhemoglobin results during vascular occlusions for two individuals (left and right) using our two-channel DOSI system. The top row shows results in the two individuals using a superficial probe with a source-detector separation of 10 mm. The bottom row shows results in the two individuals using a deep probe with a source-detector separation of 20 mm. Linear fits were performed on the deoxyhemoglobin data during the occlusions and the slope represents the magnitude of the metabolism rate ($TMRO_2$). It seems likely that the deep probe was interrogating muscle in the thinner individual and this suggests that the $TMRO_2$ of muscle tissue is >6x higher than adipose tissue.

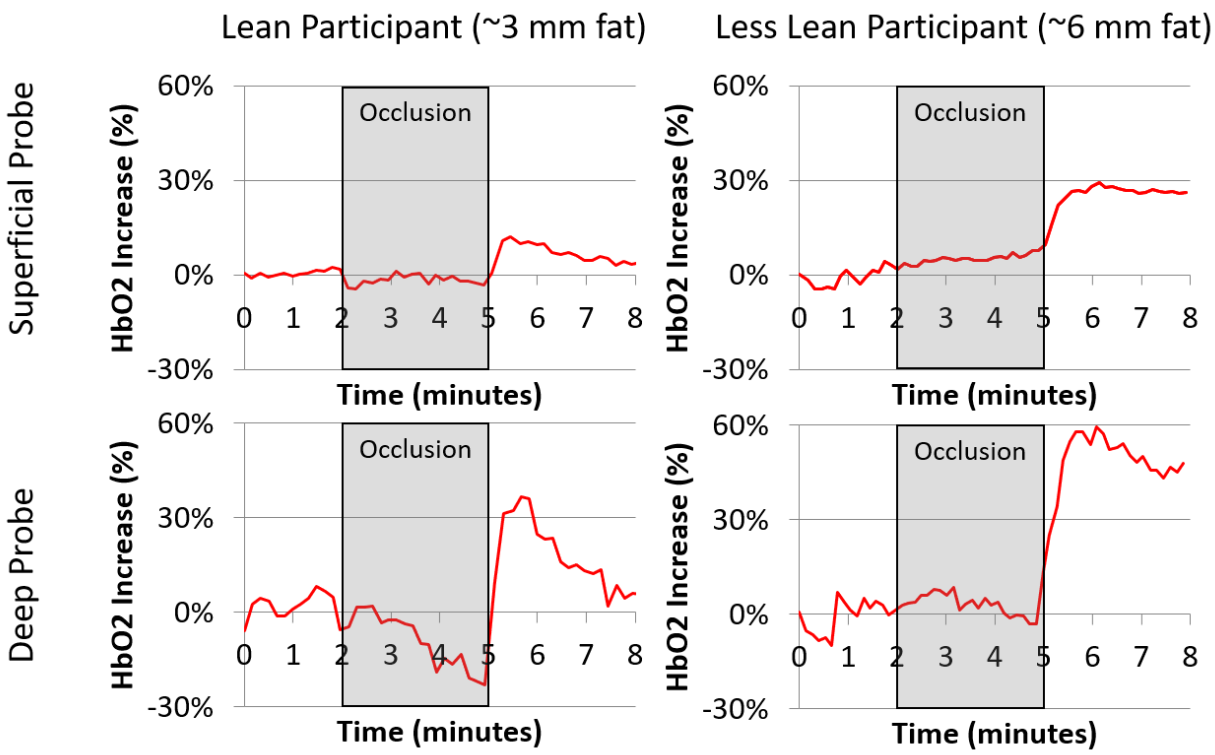

Figure 18. These plots show hyperemic responses from vascular occlusions for two individuals (left and right) using our two-channel DOSI system. The top row shows results in the two individuals using a superficial probe with a source-detector separation of 10 mm. The bottom row shows results in the two individuals using a deep probe with a source-detector separation of 20 mm. While composition and metabolism seems dependent on SATT, these results suggest that an individual's SATT will not largely affect their resulting hyperemic response. These findings agree with our results in the previous section. Source-detector separation does seem to alter the resulting hyperemic response, however, with deeper probes resulting in a greater detected hyperemic response.

4.4) Preliminary Work in Patients with Vascular Disease

The preliminary data in **Table 1** shows values for these DOSI parameters and EndoPAT's reactive hyperemia index (RHI) in a patient with endothelial dysfunction (62 yrs, female) and an age-matched, healthy control (63 yrs, female). Both participants have comparable tissue composition as indicated by the HbO_2 (~60 µM) and Hb (20-30 µM) concentrations, however, the two participants have very different metabolism and

reactivity characteristics. $TMRO_2$ is nearly 2x lower in the patient with disease and resting StO2 is higher in the patient with disease (74% vs. 65%). These two findings indicate altered tissue metabolism and such effects are expected in patients with PVD. In a recent review article by Rontoyanni et al., muscle bioenergetics in peripheral arterial disease patients is discussed and significant evidence for altered muscle oxidative capacity and altered mitochrondrial function is presented [76]. The HHR is reduced by more than 3x in the patient with disease. Previous work using other methods to assess hyperemic response such as FMD or EndoPAT have clearly demonstrated that vascular disease results in reduced hyperemic response [58]. In these two patients, an EndoPAT was also performed and the EndoPAT-derived reactive hyperemic index (RHI) is much lower in the patient with disease (1.34 vs. 1.94). Finally, the τ_{peak} and the $\tau_{relaxation}$ are shorter in the patient with disease (33 s vs. 45 s, 118 s vs. 188 s, respectively). We believe that these last parameters could be revealing information about arterial stiffness in patients. While we currently do not have arterial stiffness assessments on these preliminary participants, stiffer arteries are known to result in a faster pulse wave velocity (PWV) [60]. In future work, we will incorporate SphygmoCor to determine the relationship between the two DOSI time-based parameters and PWV.

Table 1. DOSI and EndoPAT results in healthy, age-matched control and patient with endothelial dysfunction.

Parameter Type	DOSI Parameters	DOSI Results from Participants in Figure 1		EndoPAT Parameters	EndoPAT Results from Participants in Figure 1	
		Healthy Control	Disease		Healthy Control	Disease
Metabolism	$TMRO_2$	3.1 μM/min	1.7 μM/min	NA	NA	NA
	StO_2	65%	74%			
Composition	$[HbO_2]$	63 μM	58 μM	NA	NA	NA
	[Hb]	33 μM	21 μM			
Reactivity	HHR	16%	5%	RHI	1.94	1.34
	τ_{peak}	45 s	33 s			
	$\tau_{relaxation}$	188 s	118 s			

5) CONCLUSIONS AND RECOMMENDED FUTURE WORK

The detection and management of cardiovascular disease is extremely difficult and approximately one third of patients who die from cardiovascular disease were undiagnosed or asymptomatic. We need more accurate tools which assess an array of information content, but these tools must also be cost-effective and simply to reach all sectors of the population.

Throughout this thesis, I have shown how DOSI is able to characterize a wide range of physiological phenomena which are relevant to vascular heath. DOSI can be used to study the effects of exercise and can potentially be used as a feedback mechanism when doctors prescribe lifestyle changes to patients. DOSI can also quantify tissue composition and whole-body composition in a short assessment time with a portable form factor. Obesity leads to various cardiovascular complications and tools which can accurately quantify adiposity throughout the body, including intramuscular fat, could have large impact in guiding treatment. Finally, the hemodynamic capabilities of DOSI allow for metabolic and blood flow response characterization. Many diseases can be related back to metabolism and a mismatch of

supply and demand of energy at the tissue level and the potential for a non-invasive means of assessing endothelial function could directly address the presence of “silent” cardiovascular disease that leads to death in patients that did not know they had lurking health issues.

The work in this thesis can be extended in several critical ways. First, the current form of DOSI uses FDPM instrumentation which has a ~450 MHz bandwidth for intensity modulation. In low absorbing tissues, this bandwidth is sufficient. However, the tissues which allow an assessment of an individual’s vascular health are typically much more absorbing, requiring ~1 GHz of frequency content. Our lab is currently testing and designing a network analyzer based system which allows for these higher bandwidth measurements and it should be utilized in future work in applications of this thesis. Second, the vascular occlusion studies have clearly demonstrated a sizable effect from adipose tissue. This will continue to confound hemodynamic measurements unless multi-source-detector and modeling approaches are implemented.

Finally, a quick summary of this thesis work can be summarized as follows: by studying an individual’s tissue *composition*, *metabolism*, and *vascular reactivity*, we can provide a multi-parametric assessment of their vascular health. While several optimizations are needed for each component of this assessment paradigm, a larger study should be designed where all components are assessed for a large range of patients and age-matched controls. The tests performed throughout this thesis were largely on healthy individuals and the next step will be to evaluate the dynamic range of these assessments by understanding where various disease processes place patients on each of the composition, metabolism, and vascular reactivity scales.

APPENDIX A: ACCF/AHA RECOMMENDATIONS FOR ASSESSMENT OF CVD RISK IN ASYMPTOMATIC INDIVIDUALS

The ACCF/AHA author committee scores each risk assessment technique on a 2-D grid[2]. Along one axis is an estimate of the precision of the risk assessment with scores of: A, multiple populations evaluated; B, limited populations evaluated; and C, very limited populations evaluated. The other axis is the strength of the assessment with scores of: Class I, benefit >>> risk and procedure should be performed; Class IIa, benefit >> risk and it is reasonable to perform the procedure; Class IIb, benefit ≥ risk and the procedure should be considered; and Class III, either no benefit or significant harm and the procedure should not be used. Results are summarized in the following table:

Table 3. ACCF/AHA Recommendations for CVD Risk Assessment

Risk Assessment Technique	Precision	Strength	Notes
Global Risk Scoring (e.g. Framingham Risk Score)	B	Class I	Multivariable technique that combines "classic risk factors"*
Family History	B	Class I	
Genotyping	B	Class III	
Lipoprotein & Apolipoprotein	C	Class III	
Msmt of Natriuretic Peptides	B	Class III	
Msmt of C-Reactive Protein	B	Class IIa-III	Depends on previous risk scores, age
Metabolic: Hemoglobin A1C	B	Class IIb	Predictor of diabetes
Urinary Albumin Excretion	B	Class IIa-IIb	Affected by diabetes/hypertension status
Lipoprotein-Associated Phospholipase A2	B	Class IIb	
Resting Electrocardiogram	C	Class IIa-IIb	Affected by diabetes/hypertension status
Resting Echocardiography	B-C	Class IIb-III	Affected by hypertension status
Carotid Intima-Media Size	B	Class IIa	
Brachial/Peripheral Flow-Mediated Dilation	B	Class III	
Measures of Arterial Stiffness	C	Class III	
Ankle-Brachial Index	B	Class IIa	
Exercise Electrocardiography	B	Class IIb	
Stress Echocardiography	C	Class III	
Myocardial Perfusion Imaging	C	Class IIb-III	Affected by diabetes status, family history, and previous risk scores
Computed Tomography (CT) for Coronary Calcium	B	Class IIa-III	Depends on previous risk scores
Coronary CT Angiography	C	Class III	
MRI of Plaque	C	Class III	
Special Cases: diabetes mellitus, sex, ethnicity, race, age, chronic kidney disease	See article.	See article.	See article.

*"Classic risk factors" are recognized as cigarette smoking, cholesterol levels, blood pressure levels, and diabetes status.

APPENDIX B: OPTICAL PROPERTIES OF TISSUES WITH RESPECT TO AGE

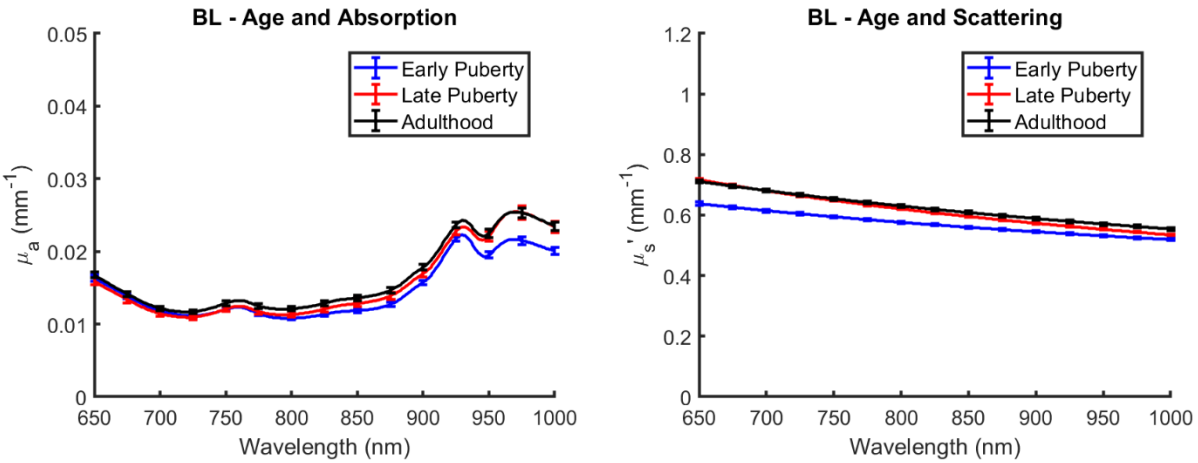

Figure 19. These plots show optical properties for the long head of the biceps (BL, outer biceps). Absorption coefficients are shown in the left plot and reduced scattering coefficients are shown in the right plot.

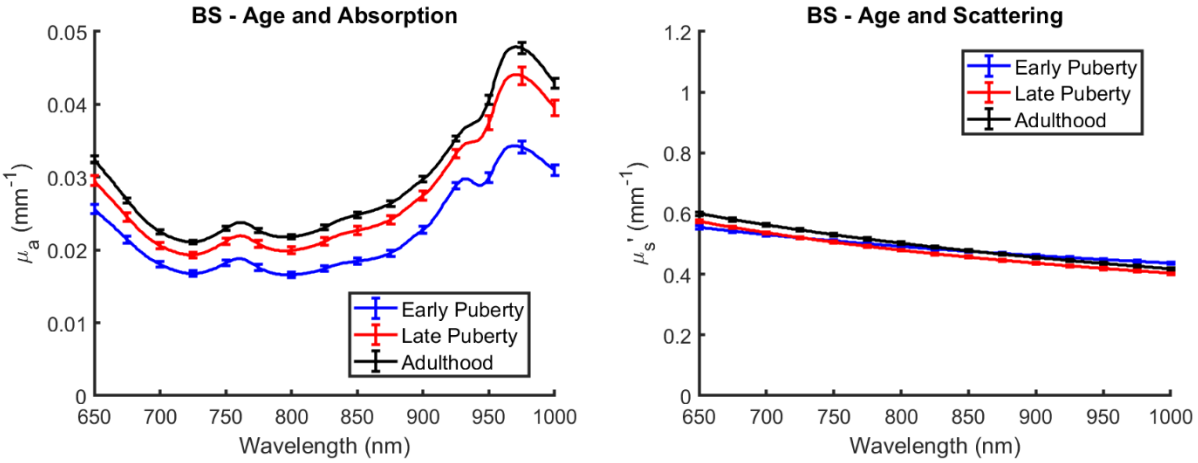

Figure 20. These plots show optical properties for the short head of the biceps (BS, inner biceps). Absorption coefficients are shown in the left plot and reduced scattering coefficients are shown in the right plot.

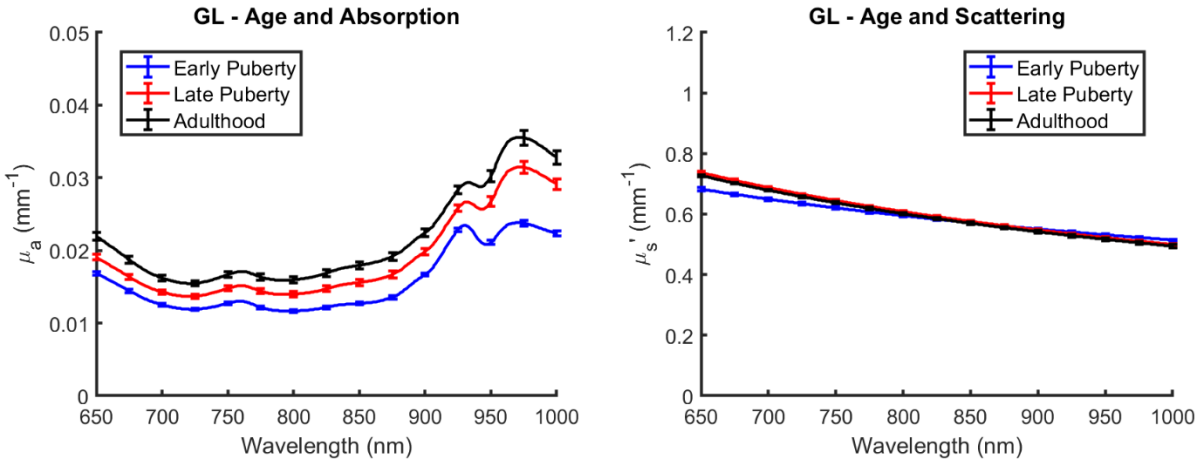

Figure 21. These plots show optical properties for the lateral head of the gastrocnemius (GL). Absorption coefficients are shown in the left plot and reduced scattering coefficients are shown in the right plot.

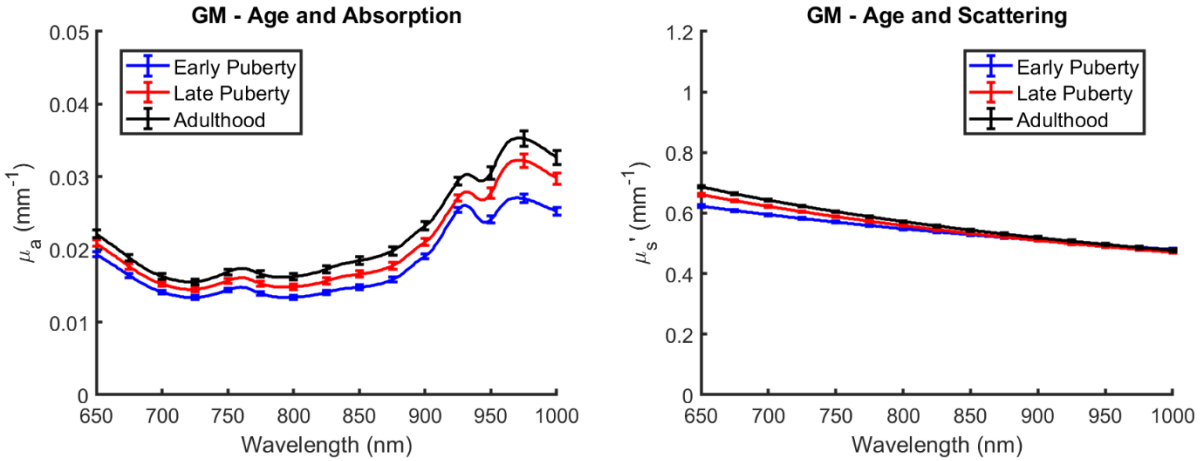

Figure 22. These plots show optical properties for the medial head of the gastrocnemius (GM). Absorption coefficients are shown in the left plot and reduced scattering coefficients are shown in the right plot.

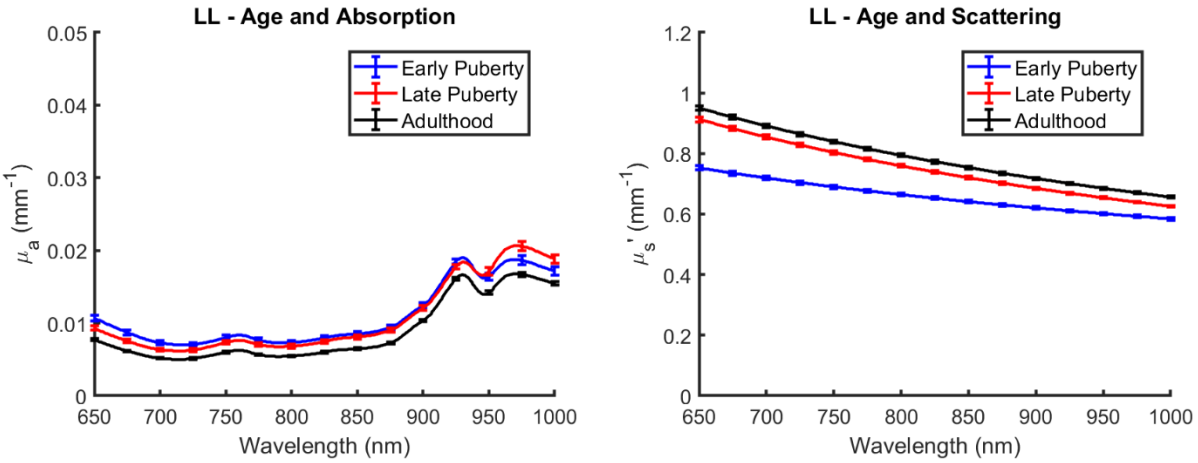

Figure 23. These plots show optical properties for the lower left abdomen (LL). Absorption coefficients are shown in the left plot and reduced scattering coefficients are shown in the right plot.

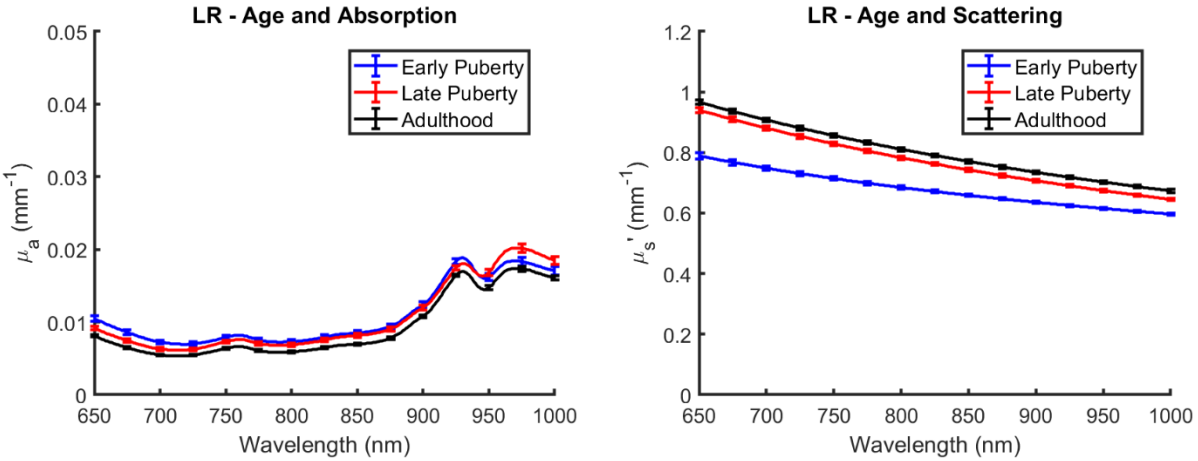

Figure 24. These plots show optical properties for the lower right abdomen (LR). Absorption coefficients are shown in the left plot and reduced scattering coefficients are shown in the right plot.

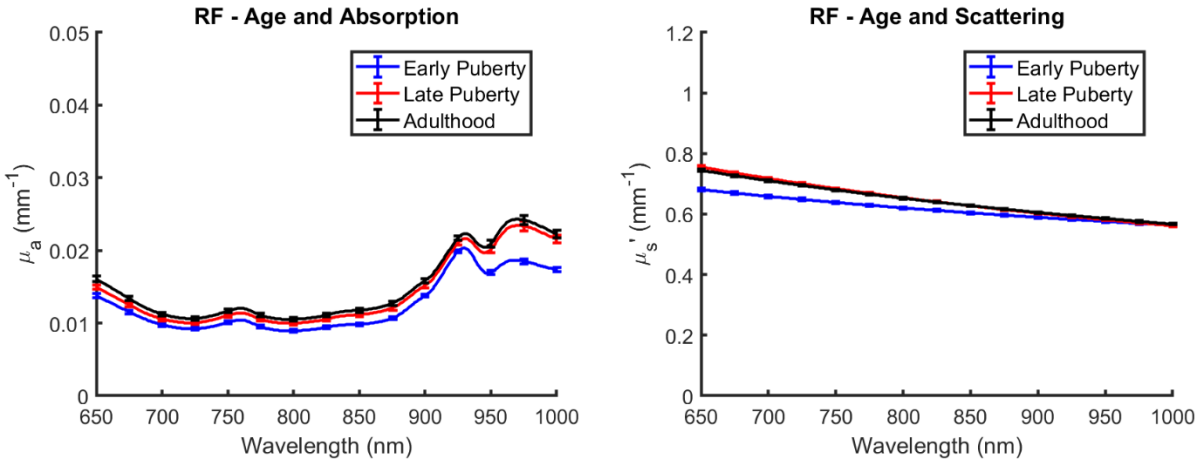

Figure 25. These plots show optical properties for the rectus femoris (RF, top of the quadriceps). Absorption coefficients are shown in the left plot and reduced scattering coefficients are shown in the right plot.

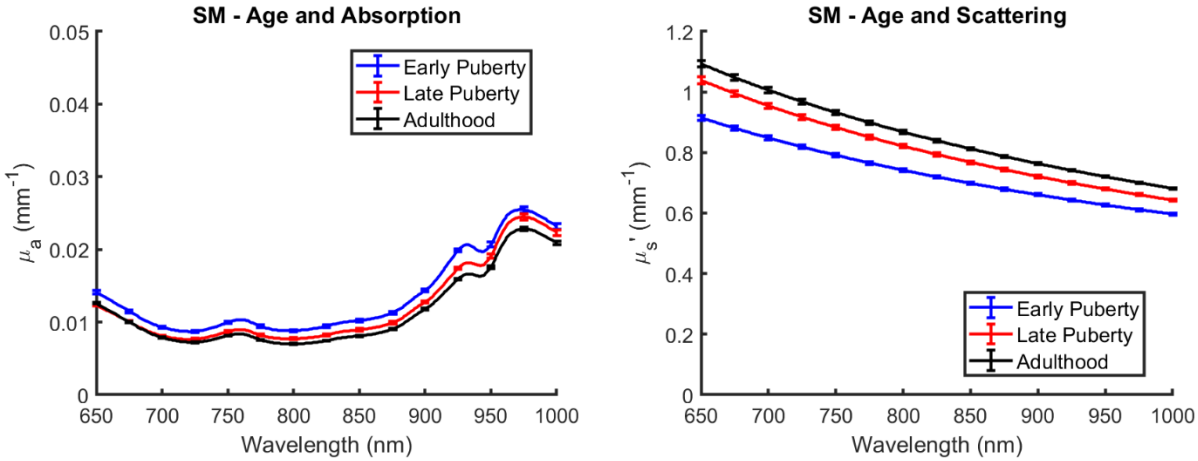

Figure 26. These plots show optical properties for the middle of the shin (SM). Absorption coefficients are shown in the left plot and reduced scattering coefficients are shown in the right plot.

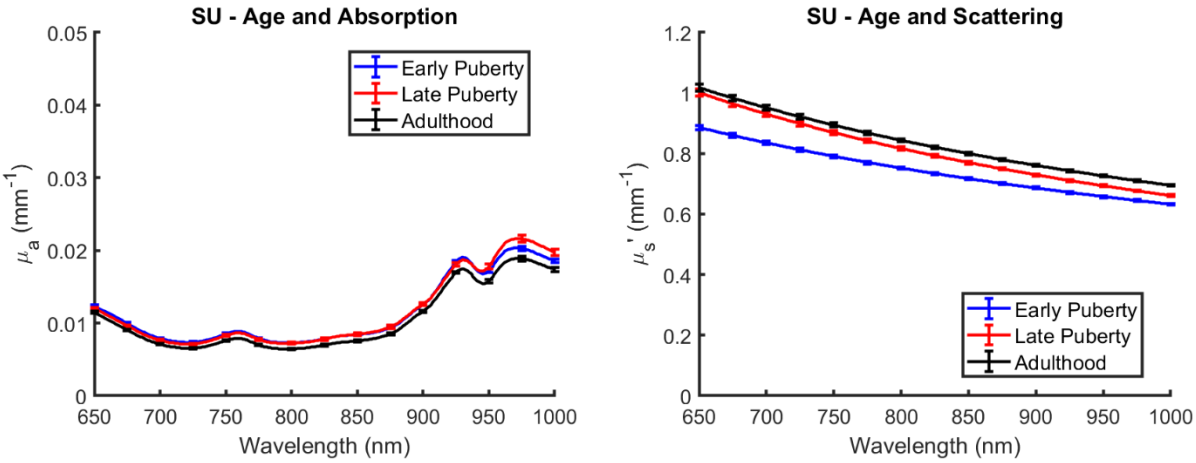

Figure 27. These plots show optical properties for the upper shin (SU). Absorption coefficients are shown in the left plot and reduced scattering coefficients are shown in the right plot.

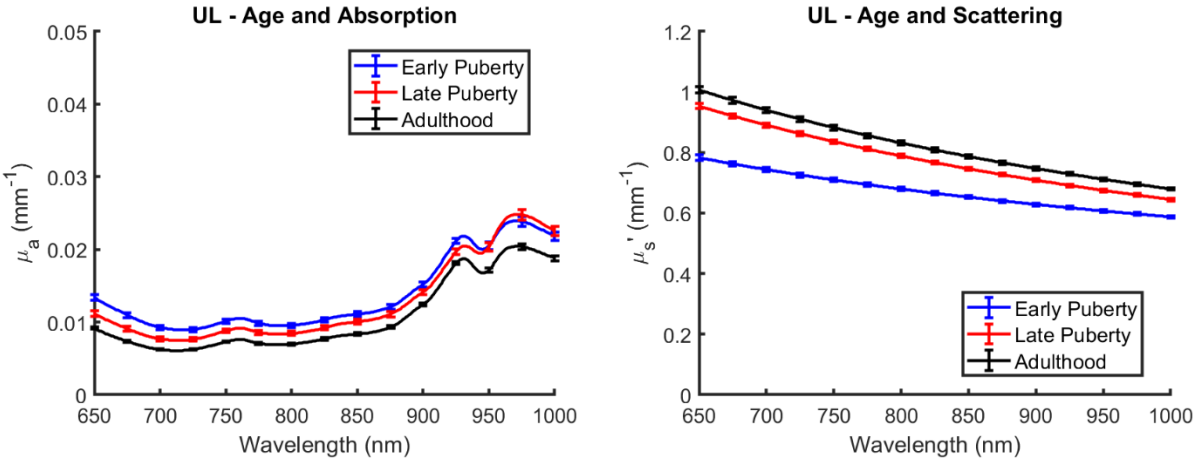

Figure 28. These plots show optical properties for the upper left abdomen (UL). Absorption coefficients are shown in the left plot and reduced scattering coefficients are shown in the right plot.

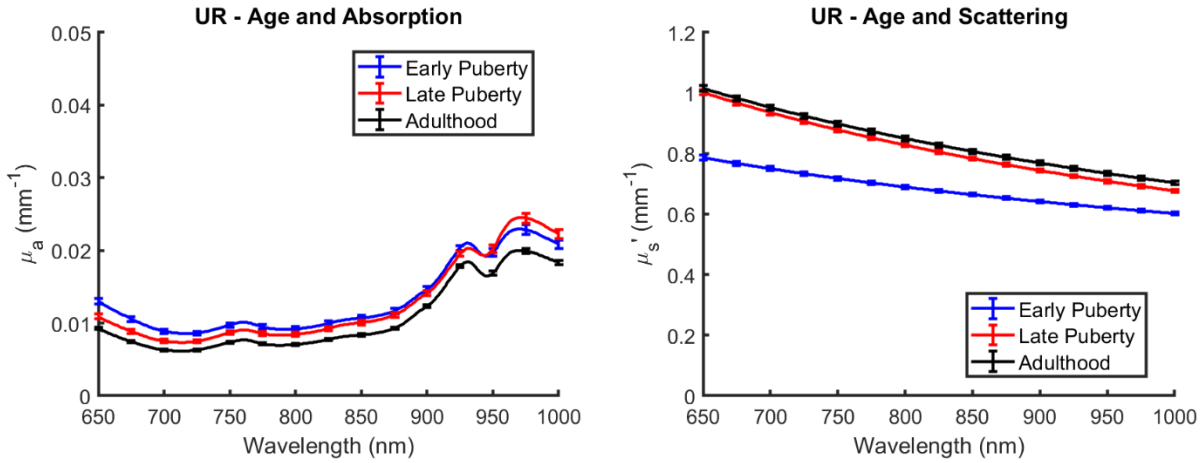

Figure 29. These plots show optical properties for the upper right abdomen (UR). Absorption coefficients are shown in the left plot and reduced scattering coefficients are shown in the right plot.

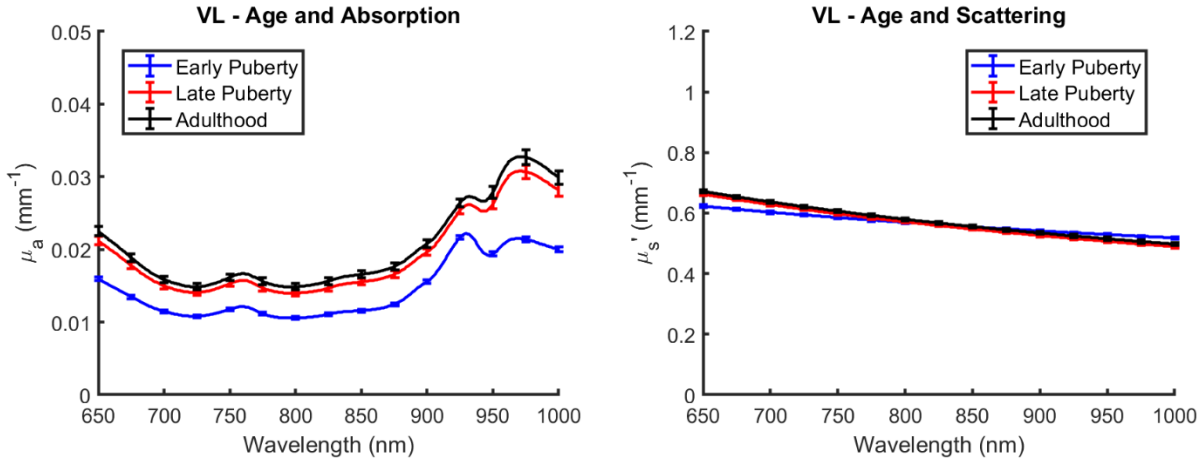

Figure 30. These plots show optical properties for the vastus lateralus (VL, side of quadriceps). Absorption coefficients are shown in the left plot and reduced scattering coefficients are shown in the right plot.

APPENDIX C: AN EMPIRICAL ADJUSTMENT TO THE DOSI DATA PROCESSING ALGORITHM

While not discussed throughout this thesis, a frequently encountered issue was low signal-to-noise ration and insufficient frequency bandwidth with certain FDPM laser diodes for accurate separation of absorption and scattering behavior. At low frequencies, phase lag increases linearly with increasing frequency but amplitude decay (or demodulation) does not significantly occur [77]. These frequency dependent behaviors are a result of the absorption and scattering properties of the tissue with higher relative levels of absorption (lower levels of scattering) increasing the critical frequency at which amplitude decay begins to take place.

In our lab, previous studies have typically focused on breast tissue which is high in scattering and low in absorption [28, 30, 78]. As these studies progressed and our DOSI technology was made more portable, hardware limitations were imposed which restrain our frequency range from 50 – 500 MHz [79]. Unfortunately, the applications discussed throughout this thesis are heavily focused on muscle and higher absorbing tissues where 450 MHz of bandwidth is too little. This loss of performance can be simulated in controlled intralipid-nigrosin phantom experiments (Figure 31).

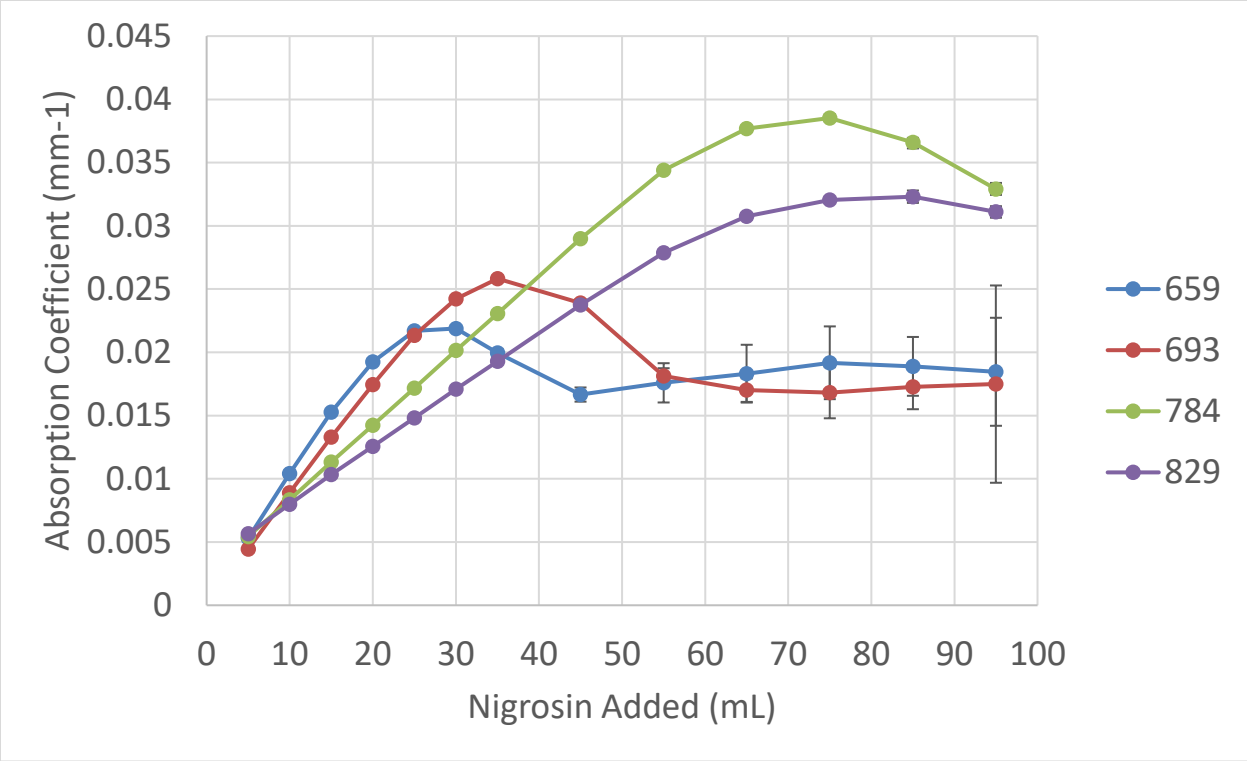

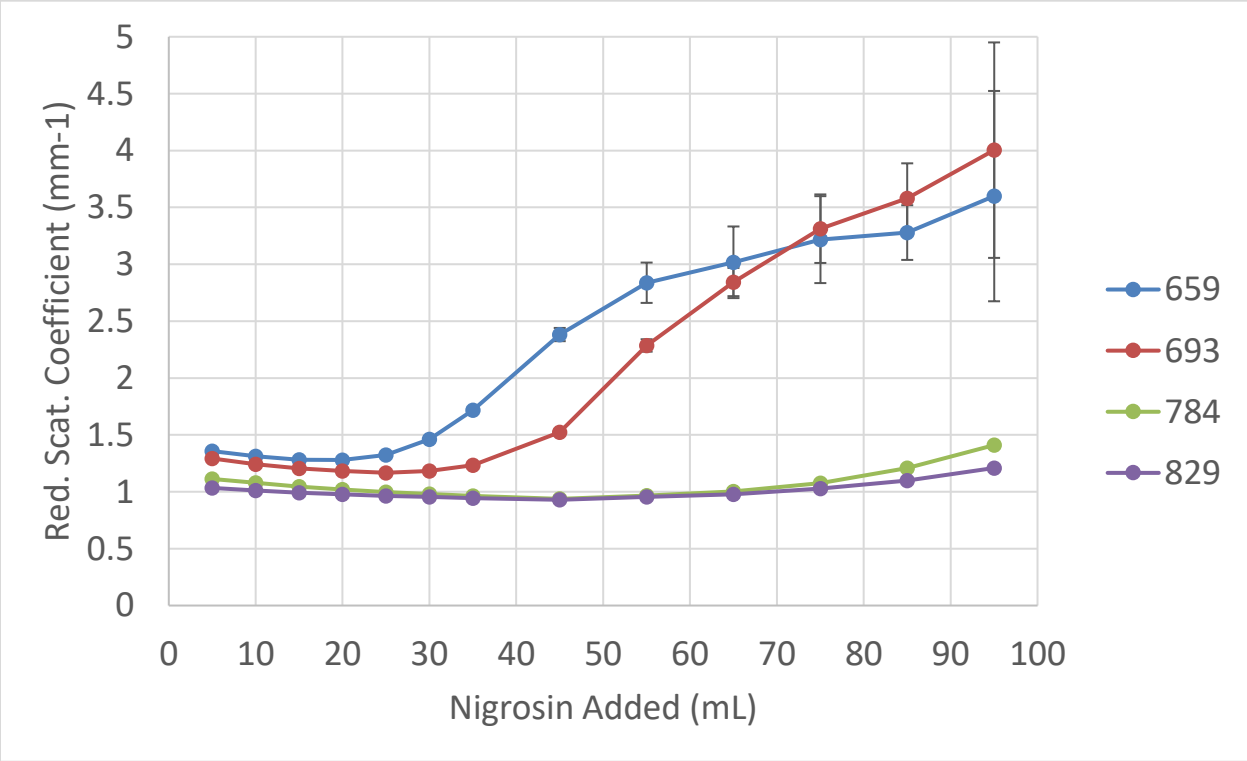

Figure 31. These plots show the results from a liquid phantom experiment. The experiment was initially composed of only intralipid (high scattering, low absorption). Nigrosin ink was added in small amounts to increase absorption. After ~25 mL of added nigrosin, absorption results are no longer accurate and erroneous absorption decreases and scattering increases are reported by FDPM.

By adding increasing levels of nigrosin to an intralipid phantom, we expected to see a linear increase in absorption and a small, linear decrease in scattering. This behavior was seen at low levels of absorption in all wavelengths of our DOSI device, but at high levels of absorption each wavelength produced erroneous results (Figure 31). However, using the large number of measurements collected throughout the body composition study, we have devised a method where we can leverage the more reliable data from the continuous-wave half of the DOSI instrument to potentially salvage problematic data that would otherwise be lost due to a failure from FDPM. In the past, this CW information content was entirely subject to the fidelity of FDPM and errors would lead to large inaccuracies when FDPM data was of poor quality, even if the CW data was of high quality.

The method works in the following steps:

1. Select reliable FDPM wavelengths which can accurately separate absorption and scattering.
2. Calculate $\mu_a(\lambda)$ and $\mu_s'(\lambda)$ at the FDPM wavelengths.
3. Use the $\mu_a(\lambda)$ data from the FDPM wavelengths to calculate only the concentrations of oxy- and deoxy-hemoglobin. (Note: at this step, we expect FDPM-derived hemoglobin concentrations to have lower accuracy.)
4. Use the CW method described above to calculate water and fat content.
5. Sum the component absorption spectra for each chromophore (oxy- and deoxy-hemoglobin as calculated from FDPM and water and fat as calculated from the CW method) to obtain a broadband $\mu_a(\lambda)$ spectrum.

6. Utilize the CW reflectance spectrum and the $\mu_a(\lambda)$ spectrum derived in step 5 to calculate $\mu_s'(\lambda)$ coefficients at 930 and 970 nm (wavelengths used to calculate fat and water content).
7. Fit FDPM-derived reduced scattering coefficients and the two reduced scattering coefficients derived in step 6 at 930 and 970 nm to the expected power law from Mie theory.
8. Utilize the broadband $\mu_s'(\lambda)$ derived in step 7 and the CW reflectance to calculate a broadband $\mu_a(\lambda)$ spectrum.
9. Use the broadband $\mu_a(\lambda)$ spectrum from step 8 to solve for component spectra and chromophore concentrations.
10. Carry forward the oxy- and deoxy-hemoglobin concentrations from step 8 then repeat steps 3 – 8 once more to obtain final chromophore concentrations.

REFERENCES

[1] H. Ni *et al.*, "Trends from 1987 to 2004 in sadden death due to coronary heart disease: The Atherosclerosis Risk in Communities (ARIC) study," (in English), *American Heart Journal,* Article vol. 157, no. 1, pp. 46-52, Jan 2009.

[2] P. Greenland *et al.*, "2010 AACF/AHA Guideline for Assessment of Cardiovascular Risk in Asymptomatic Adults," *Circulation,* vol. 122, pp. 584-636, 2010.

[3] WHO, "The top 10 causes of death," *World Health Organization,* Accessed on: JulyAvailable: http://www.who.int/mediacentre/factsheets/fs310/en/index.html

[4] H. Eyre, R. Kahn, and R. M. Robertson, "Preventing Cancer, Cardiovascular Disease, and Diabetes," *Diabetes Care,* vol. 27, no. 7, pp. 1812-1824, 2004.

[5] S. L. Jacques, "Optical Properties of Biological Tissues: A Review," *Phys. Med. Biol.,* vol. 58, pp. 37-61, 2013.

[6] R. Haskell, L. Svaasand, T. Tsay, T. Feng, M. McAdams, and B. Tromberg, "Boundary Equations for the Diffusion Equation in Radative Transfer," *Journal of the Optical Society of America A,* vol. 11, no. 10, pp. 2727-2741, 1994.

[7] T. D. O'Sullivan, A. E. Cerussi, D. J. Cuccia, and B. J. Tromberg, "Diffuse optical imaging using spatially and temporally modulated light," (in English), *Journal of Biomedical Optics,* Article vol. 17, no. 7, p. 14, Jul 2012, Art. no. 071311.

[8] F. Bevilacqua, A. J. Berger, A. E. Cerussi, D. Jakubowski, and B. J. Tromberg, "Broadband absorption spectroscopy in turbid media by combined frequency-domain and steady-state methods," (in English), *Applied Optics,* Article vol. 39, no. 34, pp. 6498-6507, Dec 2000.

[9] P. Felig, "GLUCOSE-ALANINE CYCLE," (in English), *Metabolism-Clinical and Experimental,* Article vol. 22, no. 2, pp. 179-207, 1973.

[10] T. C. Bonne *et al.*, ""Live High-Train High" increases hemoglobin mass in Olympic swimmers," (in English), *European Journal of Applied Physiology,* Article vol. 114, no. 7, pp. 1439-1449, Jul 2014.

[11] C. T. Pereira *et al.*, "Age-dependent differences in survival after severe burns: A unicentric review of 1,674 patients and 179 autopsies over 15 years," (in English), *Journal of the American College of Surgeons,* Article; Proceedings Paper vol. 202, no. 3, pp. 536-548, Mar 2006.

[12] R. R. Wolfe, "The underappreciated role of muscle in health and disease," (in English), *American Journal of Clinical Nutrition,* Review vol. 84, no. 3, pp. 475-482, Sep 2006.

[13] A. Pietrobelli, C. Formica, Z. M. Wang, and S. B. Heymsfield, "Dual-energy X-ray absorptiometry body composition model: Review of physical concepts," (in English), *American Journal of Physiology-Endocrinology and Metabolism,* Review vol. 271, no. 6, pp. E941-E951, Dec 1996.

[14] M. Ferrari, T. Binzoni, and V. Quaresima, "Oxidative metabolism in muscle," (in English), *Philosophical Transactions of the Royal Society of London Series B-Biological Sciences,* Article; Proceedings Paper vol. 352, no. 1354, pp. 677-683, Jun 1997.

[15] M. I. R. Pereira, P. S. C. Gomes, and Y. N. Bhambhani, "A brief review of the use of near infrared spectroscopy with particular interest in resistance exercise," (in English), *Sports Medicine,* Review vol. 37, no. 7, pp. 615-624, 2007.
[16] M. Wolf, M. Ferrari, and V. Quaresima, "Progress of near-infrared spectroscopy and topography for brain and muscle clinical applications," (in English), *Journal of Biomedical Optics,* Review vol. 12, no. 6, p. 14, Nov-Dec 2007, Art. no. 062104.
[17] B. Chance *et al.*, "TIME-RESOLVED SPECTROSCOPY OF HEMOGLOBIN AND MYOGLOBIN IN RESTING AND ISCHEMIC MUSCLE," (in English), *Analytical Biochemistry,* Article vol. 174, no. 2, pp. 698-707, Nov 1988.
[18] A. Torricelli *et al.*, "Mapping of calf muscle oxygenation and haemoglobin content during dynamic plantar flexion exercise by multi-channel time-resolved near-infrared spectroscopy," (in English), *Physics in Medicine and Biology,* Article vol. 49, no. 5, pp. 685-699, Mar 2004, Art. no. Pii s0031-9155(04)66557-2.
[19] U. Wolf, M. Wolf, J. H. Choi, A. Paunescu, A. Michalos, and E. Gratton, "Regional differences of Hemodynamics and oxygenation in the human calf muscle detected with near-infrared spectrophotometry," (in English), *Journal of Vascular and Interventional Radiology,* Article vol. 18, no. 9, pp. 1094-1101, Sep 2007.
[20] B. Henry *et al.*, "Hybrid diffuse optical techniques for continuous hemodynamic measurement in gastrocnemius during plantar flexion exercise," (in English), *Journal of Biomedical Optics,* Article vol. 20, no. 12, p. 10, Dec 2015, Art. no. 125006.
[21] G. Q. Yu *et al.*, "Time-dependent blood flow and oxygenation in human skeletal muscles measured with noninvasive near-infrared diffuse optical spectroscopies," (in English), *Journal of Biomedical Optics,* Article vol. 10, no. 2, p. 12, Mar-Apr 2005, Art. no. 024027.
[22] G. Ganesan *et al.*, "Diffuse optical spectroscopic imaging of subcutaneous adipose tissue metabolic changes during weight loss," (in English), *International Journal of Obesity,* Article vol. 40, no. 8, pp. 1292-1300, Aug 2016.
[23] T. Moritani and H. A. Devries, "NEURAL FACTORS VERSUS HYPERTROPHY IN THE TIME COURSE OF MUSCLE STRENGTH GAIN," (in English), *American Journal of Physical Medicine & Rehabilitation,* Article vol. 58, no. 3, pp. 115-130, 1979.
[24] R. S. Staron *et al.*, "SKELETAL-MUSCLE ADAPTATIONS DURING EARLY PHASE OF HEAVY-RESISTANCE TRAINING IN MEN AND WOMEN," (in English), *Journal of Applied Physiology,* Article vol. 76, no. 3, pp. 1247-1255, Mar 1994.
[25] J. M. DeFreitas, T. W. Beck, M. S. Stock, M. A. Dillon, and P. R. Kasishke, "An examination of the time course of training-induced skeletal muscle hypertrophy," (in English), *European Journal of Applied Physiology,* Article vol. 111, no. 11, pp. 2785-2790, Nov 2011.
[26] O. R. Seynnes, M. de Boer, and M. V. Narici, "Early skeletal muscle hypertrophy and architectural changes in response to high-intensity resistance training," (in English), *Journal of Applied Physiology,* Article vol. 102, no. 1, pp. 368-373, Jan 2007.

[27] F. Damas *et al.*, "Early resistance training-induced increases in muscle cross-sectional area are concomitant with edema-induced muscle swelling," (in English), *European Journal of Applied Physiology,* Article vol. 116, no. 1, pp. 49-56, Jan 2016.
[28] A. Cerussi *et al.*, "Predicting response to breast cancer neoadjuvant chemotherapy using diffuse optical spectroscopy," (in English), *Proceedings of the National Academy of Sciences of the United States of America,* Article vol. 104, no. 10, pp. 4014-4019, Mar 2007.
[29] D. B. Jakubowski *et al.*, "Monitoring neoadjuvant chemotherapy in breast cancer using quantitative diffuse optical spectroscopy: a case study," (in English), *Journal of Biomedical Optics,* Article vol. 9, no. 1, pp. 230-238, Jan-Feb 2004.
[30] B. J. Tromberg *et al.*, "Predicting Responses to Neoadjuvant Chemotherapy in Breast Cancer: ACRIN 6691 Trial of Diffuse Optical Spectroscopic Imaging," (in English), *Cancer Research,* Article vol. 76, no. 20, pp. 5933-5944, Oct 2016.
[31] S. Merritt *et al.*, "Comparison of water and lipid content measurements using diffuse optical spectroscopy and MRI in emulsion phantoms," (in English), *Technology in Cancer Research & Treatment,* Article vol. 2, no. 6, pp. 563-569, Dec 2003.
[32] T. Baechle, R. Earle, and D. Wathen, "Resistance Training," in *Essentials of Strength Training and Conditioning*Champaign, IL: Human Kinetics, 2008, pp. 381-412.
[33] R. B. Rusu, S. Cousins, and Ieee, "3D is here: Point Cloud Library (PCL)," in *IEEE International Conference on Robotics and Automation (ICRA)*, Shanghai, PEOPLES R CHINA, 2011, NEW YORK: Ieee, 2011.
[34] J. M. Bland and D. G. Altman, "CALCULATING CORRELATION-COEFFICIENTS WITH REPEATED OBSERVATIONS .2. CORRELATION BETWEEN SUBJECTS," (in English), *British Medical Journal,* Note vol. 310, no. 6980, pp. 633-633, Mar 1995.
[35] M. Ferrari, M. Muthalib, and V. Quaresima, "The use of near-infrared spectroscopy in understanding skeletal muscle physiology: recent developments," *Philosophical Transactions of the Royal Society a-Mathematical Physical and Engineering Sciences,* vol. 369, no. 1955, pp. 4577-4590, Nov 2011.
[36] M. L. Davis and T. J. Barstow, "Estimated contribution of hemoglobin and myoglobin to near infrared spectroscopy," (in English), *Respiratory Physiology & Neurobiology,* Article vol. 186, no. 2, pp. 180-187, Apr 2013.
[37] D. J. Marcinek, C. E. Amara, K. Matz, K. E. Conley, and K. A. Schenkman, "Wavelength shift analysis: A simple method to determine the contribution of hemoglobin and myoglobin to in vivo optical spectra," (in English), *Applied Spectroscopy,* Article vol. 61, no. 6, pp. 665-669, Jun 2007.
[38] E. Ohmae *et al.*, "Sensitivity correction for the influence of the fat layer on muscle oxygenation and estimation of fat thickness by time-resolved spectroscopy," (in English), *Journal of Biomedical Optics,* Article vol. 19, no. 6, p. 11, Jun 2014, Art. no. 067005.
[39] T. E. Ryan, W. M. Southern, J. T. Brizendine, and K. K. McCully, "Activity-Induced Changes in Skeletal Muscle Metabolism Measured with Optical

Spectroscopy," (in English), *Medicine and Science in Sports and Exercise,* Article vol. 45, no. 12, pp. 2346-2352, Dec 2013.
[40] T. K. Tran *et al.*, "Comparative analysis of NMR and NIRS measurements of intracellular PO2 in human skeletal muscle," (in English), *American Journal of Physiology-Regulatory Integrative and Comparative Physiology,* Article vol. 276, no. 6, pp. R1682-R1690, Jun 1999.
[41] J. R. Wilson, D. M. Mancini, K. McCully, N. Ferraro, V. Lanoce, and B. Chance, "NONINVASIVE DETECTION OF SKELETAL-MUSCLE UNDERPERFUSION WITH NEAR-INFRARED SPECTROSCOPY IN PATIENTS WITH HEART-FAILURE," (in English), *Circulation,* Article vol. 80, no. 6, pp. 1668-1674, Dec 1989.
[42] B. R. McKay, D. H. Paterson, and J. M. Kowalchuk, "Effect of short-term high-intensity interval training vs. continuous training on O-2 uptake kinetics, muscle deoxygenation, and exercise performance," (in English), *Journal of Applied Physiology,* Article vol. 107, no. 1, pp. 128-138, Jul 2009.
[43] N. Lai *et al.*, "Modeling oxygenation in venous blood and skeletal muscle in response to exercise using near-infrared spectroscopy," (in English), *Journal of Applied Physiology,* Article vol. 106, no. 6, pp. 1858-1874, Jun 2009.
[44] D. M. Mancini, L. Bolinger, H. Li, K. Kendrick, B. Chance, and J. R. Wilson, "VALIDATION OF NEAR-INFRARED SPECTROSCOPY IN HUMANS," (in English), *Journal of Applied Physiology,* Article vol. 77, no. 6, pp. 2740-2747, Dec 1994.
[45] K. Masuda, T. Yamada, R. Ishizawa, and H. Takakura, "Role of myoglobin in regulating respiration
during muscle contraction," *J Phys Fitness Sports Med,* vol. 2, no. 1, pp. 9-16, 2013.
[46] G. K. Stebbings, C. I. Morse, G. E. McMahon, and G. L. Onambele, "Resting Arterial Diameter and Blood Flow Changes With Resistance Training and Detraining in Healthy Young Individuals," (in English), *Journal of Athletic Training,* Article vol. 48, no. 2, pp. 209-219, Mar-Apr 2013.
[47] P. A. Tesch, A. Thorsson, and P. Kaiser, "MUSCLE CAPILLARY SUPPLY AND FIBER TYPE CHARACTERISTICS IN WEIGHT AND POWER LIFTERS," (in English), *Journal of Applied Physiology,* Article vol. 56, no. 1, pp. 35-38, 1984.
[48] G. E. R. Campos *et al.*, "Muscular adaptations in response to three different resistance-training regimens: specificity of repetition maximum training zones," (in English), *European Journal of Applied Physiology,* Article vol. 88, no. 1-2, pp. 50-60, Nov 2002.
[49] B. M. Hather, P. A. Tesch, P. Buchanan, and G. A. Dudley, "INFLUENCE OF ECCENTRIC ACTIONS ON SKELETAL-MUSCLE ADAPTATIONS TO RESISTANCE TRAINING," (in English), *Acta Physiologica Scandinavica,* Article vol. 143, no. 2, pp. 177-185, Oct 1991.
[50] M. Ng *et al.*, "Global, regional, and national prevalence of overweight and obesity in children and adults during 1980-2013: a systematic analysis for the Global Burden of Disease Study 2013," (in English), *Lancet,* Article vol. 384, no. 9945, pp. 766-781, Aug 2014.
[51] C. J. Lavie, R. V. Milani, and H. O. Ventura, "Obesity and Cardiovascular Disease Risk Factor, Paradox, and Impact of Weight Loss," (in English), *Journal*

of the American College of Cardiology, Article vol. 53, no. 21, pp. 1925-1932, May 2009.
[52] G. Whitlock *et al.*, "Body-mass index and cause-specific mortality in 900 000 adults: collaborative analyses of 57 prospective studies," (in English), *Lancet,* Article vol. 373, no. 9669, pp. 1083-1096, Mar-Apr 2009.
[53] R. Loeppke, M. Taitel, V. Haufle, T. Parry, R. C. Kessler, and K. Jinnett, "Health and Productivity as a Business Strategy: A Multiemployer Study," (in English), *Journal of Occupational and Environmental Medicine,* Article vol. 51, no. 4, pp. 411-428, Apr 2009.
[54] A. G. Tsai, D. F. Williamson, and H. A. Glick, "Direct medical cost of overweight and obesity in the USA: a quantitative systematic review," (in English), *Obesity Reviews,* Review vol. 12, no. 1, pp. 50-61, Jan 2011.
[55] D. M. Cooper, S. Y. Leu, P. Galassetti, and S. Radom-Aizik, "Dynamic Interactions of Gas Exchange, Body Mass, and Progressive Exercise in Children," (in English), *Medicine and Science in Sports and Exercise,* Article vol. 46, no. 5, pp. 877-886, May 2014.
[56] O. Addison, R. L. Marcus, P. C. LaStayo, and A. S. Ryan, "Intermuscular Fat: A Review of the Consequences and Causes," (in English), *International Journal of Endocrinology,* Review p. 11, 2014, Art. no. 309570.
[57] J. M. Conway, K. H. Norris, and C. E. Bodwell, "A NEW APPROACH FOR THE ESTIMATION OF BODY-COMPOSITION - INFRARED INTERACTANCE," (in English), *American Journal of Clinical Nutrition,* Article vol. 40, no. 6, pp. 1123-1130, 1984.
[58] J. E. Deanfield, J. P. Halcox, and T. J. Rabelink, "Endothelial function and dysfunction: testing and clinical relevance," (in eng), *Circulation,* vol. 115, no. 10, pp. 1285-95, Mar 2007.
[59] M. E. Widlansky, N. Gokce, J. F. Keaney, and J. A. Vita, "The clinical implications of endothelial dysfunction," (in eng), *J Am Coll Cardiol,* vol. 42, no. 7, pp. 1149-60, Oct 2003.
[60] T. J. Anderson, "Arterial stiffness or endothelial dysfunction as a surrogate marker of vascular risk," (in eng), *Can J Cardiol,* vol. 22 Suppl B, pp. 72B-80B, Feb 2006.
[61] I. B. Wilkinson and C. M. McEniery, "Arterial stiffness, endothelial function and novel pharmacological approaches," (in eng), *Clin Exp Pharmacol Physiol,* vol. 31, no. 11, pp. 795-9, Nov 2004.
[62] R. Rubinshtein *et al.*, "Assessment of endothelial function by non-invasive peripheral arterial tonometry predicts late cardiovascular adverse events," (in eng), *Eur Heart J,* vol. 31, no. 9, pp. 1142-8, May 2010.
[63] J. Yeboah, J. R. Crouse, F. C. Hsu, G. L. Burke, and D. M. Herrington, "Brachial flow-mediated dilation predicts incident cardiovascular events in older adults: the Cardiovascular Health Study," (in eng), *Circulation,* vol. 115, no. 18, pp. 2390-7, May 2007.
[64] S. Laurent *et al.*, "Aortic stiffness is an independent predictor of fatal stroke in essential hypertension," (in eng), *Stroke,* vol. 34, no. 5, pp. 1203-6, May 2003.

[65] W. W. Nichols and B. M. Singh, "Augmentation index as a measure of peripheral vascular disease state," (in eng), *Curr Opin Cardiol,* vol. 17, no. 5, pp. 543-51, Sep 2002.
[66] R. A. De Blasi, M. Cope, C. Elwell, F. Safoue, and M. Ferrari, "Noninvasive measurement of human forearm oxygen consumption by near infrared spectroscopy," (in eng), *Eur J Appl Physiol Occup Physiol,* vol. 67, no. 1, pp. 20-5, 1993.
[67] T. Hamaoka *et al.*, "Noninvasive measures of oxidative metabolism on working human muscles by near-infrared spectroscopy," (in eng), *J Appl Physiol (1985),* vol. 81, no. 3, pp. 1410-7, Sep 1996.
[68] R. Kragelj, T. Jarm, T. Erjavec, M. Presern-Strukelj, and D. Miklavcic, "Parameters of postocclusive reactive hyperemia measured by near infrared spectroscopy in patients with peripheral vascular disease and in healthy volunteers," (in eng), *Ann Biomed Eng,* vol. 29, no. 4, pp. 311-20, Apr 2001.
[69] R. A. De Blasi *et al.*, "Microvascular dysfunction and skeletal muscle oxygenation assessed by phase-modulation near-infrared spectroscopy in patients with septic shock," (in eng), *Intensive Care Med,* vol. 31, no. 12, pp. 1661-8, Dec 2005.
[70] Z. S. Hosseini, E. Zahedi, H. Movahedian Attar, H. Fakhrzadeh, and M. H. Parsafar, "Discrimination between different degrees of coronary artery disease using time-domain features of the finger photoplethysmogram in response to reactive hyperemia," *Biomedical Signal Processing and Control,* vol. 18, pp. 282-292, 2015.
[71] B. J. Tromberg, A. E. Cerussi, S.-H. Chung, W. Tanamai, and A. Durkin, "Broadband diffuse optical spectroscopic imaging," in *Handbook of Biomedical Optics*, C. P. David A. Boas, Nimmi Ramanujuam, Ed.: CRC Press, 2011, p. 181.
[72] T. D. O'Sullivan, A. E. Cerussi, D. J. Cuccia, and B. J. Tromberg, "Diffuse optical imaging using spatially and temporally modulated light," (in eng), *J Biomed Opt,* vol. 17, no. 7, p. 071311, Jul 2012.
[73] T. O'Sullivan, A. Cerussi, D. Cuccia, and B. Tromberg, "Diffuse optical imaging using spatially and temporally modulated light," *Journal of Biomedical Optics,* vol. 17, no. 7, 2012.
[74] H. S. Yazdi *et al.*, "Mapping breast cancer blood flow index, composition, and metabolism in a human subject using combined diffuse optical spectroscopic imaging and diffuse correlation spectroscopy," (in English), *Journal of Biomedical Optics,* Article vol. 22, no. 4, p. 10, Apr 2017, Art. no. 045003.
[75] M. Niwayama, L. Lin, J. Shao, N. Kudo, and K. Yamamoto, "Quantitative measurement of muscle hemoglobin oxygenation using near-infrared spectroscopy with correction for the influence of a subcutaneous fat layer," (in English), *Review of Scientific Instruments,* Article vol. 71, no. 12, pp. 4571-4575, Dec 2000, Art. no. Pii [s0034-6748(00)02812-4].
[76] V. G. Rontoyanni, O. Nunez Lopez, G. T. Fankhauser, Z. F. Cheema, B. B. Rasmussen, and C. Porter, "Mitochondrial Bioenergetics in the Metabolic Myopathy Accompanying Peripheral Artery Disease," (in eng), *Front Physiol,* vol. 8, p. 141, 2017.

[77] B. J. Tromberg, L. O. Svaasand, T. T. Tsay, and R. C. Haskell, "Properties of photon density waves in multiple-scattering media," (in English), *Applied Optics,* Article vol. 32, no. 4, pp. 607-616, Feb 1993.
[78] A. E. Cerussi, V. W. Tanamai, D. Hsiang, J. Butler, R. S. Mehta, and B. J. Tromberg, "Diffuse optical spectroscopic imaging correlates with final pathological response in breast cancer neoadjuvant chemotherapy," (in English), *Philosophical Transactions of the Royal Society a-Mathematical Physical and Engineering Sciences,* Article vol. 369, no. 1955, pp. 4512-4530, Nov 2011.
[79] K. S. No, R. Kwong, P. H. Chou, and A. Cerussi, "Design and testing of a miniature broadband frequency domain photon migration instrument," (in English), *Journal of Biomedical Optics,* Article vol. 13, no. 5, p. 3, Sep-Oct 2008, Art. no. 050509.